Title

Conditioner for a Helically Transported Electron Beam

Author

Wang, C

Publication Date

1992-05-01

LBL-32222
UC-414

Lawrence Berkeley Laboratory
UNIVERSITY OF CALIFORNIA

Accelerator & Fusion
Research Division

Conditioner for a Helically Transported Electron Beam

C. Wang

May 1992

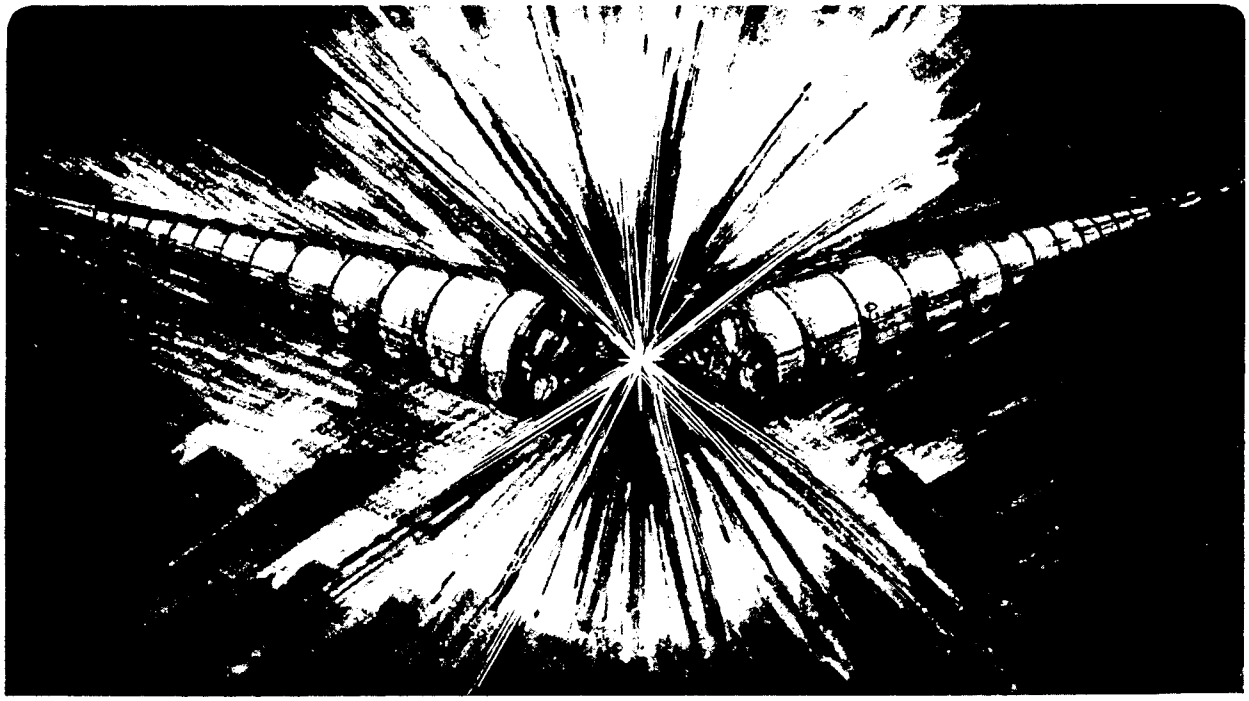

Prepared for the U.S. Department of Energy under Contract Number DE-AC03-76SF00098

DISCLAIMER

LBL-32222
ESG - 182
UC-414

Conditioner for a Helically Transported Electron Beam*

Changbiao Wang**

Lawrence Berkeley Laboratory, University of California, Berkeley, California 94720

May 1992

* Work supported by the Director, Office of Energy Research, Office of High Energy and Nuclear Physics, Division of High Energy Physics, of the U.S. Department of Energy under Contract No. DE-AC03-76SF00098

** On leave from University of Electronic Science and Technology of China, Chengdu, Sichuan, 610054, China

CONDITIONER FOR A HELICALLY TRANSPORTED ELECTRON BEAM**

Changbiao Wang*
Lawrence Berkeley Laboratory
University of California
Berkeley, CA 94720

May 8, 1992

ABSTRACT

The kinetic theory is developed to investigate a conditioner for a helically transported electron beam. Linear expressions for axial velocity spread are derived. Numerical simulation is used to check the theoretical results and examine nonlinear aspects of the conditioning process. The results show that in the linear regime the action of the beam conditioner on a pulsed beam mainly depends on the phase at which the beam enters the conditioner and depends only slightly on the operating wavelength. In the nonlinear regime, however, the action of the conditioner strongly depends on the operating wavelength and only slightly upon the entrance phase. For a properly chosen operating wavelength, a little less than the electron's relativistic cyclotron wavelength, the conditioner can decrease the axial velocity spread of a pulsed beam down to less than one-third of its initial value.

* On leave from University of Electronic Science and Technology of China, Chengdu, Sichuan, 610054, China

** Work supported by the Director, Office of Energy Research, Office of High Energy and Nuclear Physics, Division of High Energy Physics, of the U.S. Department of Energy under Contract Number DE-AC03-76SF00098

I. Introduction

In a beam conditioner, proposed by Sessler, Whittum and Yu,[1,2,3] a nearly monoenergetic beam has the shape of the beam's phase volume so changed that its axial velocity spread is improved. As a result, the beam conditioner can greatly reduce the spread in axial velocity of an electron beam, and hence it can be used, with advantage, on almost all fast wave devices. It is therefore natural that it has aroused considerable attention.[4,5]

There are different means for conditioning electron beams. The longitudinal electric field in a microwave cavity, as proposed by Sessler, et al, can be used to condition electron beams, and this is an efficient method. However, for low energy beams, transported by a helical magnetic field, some other method of beam conditioning is required. The transverse electric field in an RF cavity can, conveniently, be used for this purpose.

In this paper, we present a kinetic formulation of a conditioner consisting of a microwave cavity operating in the TE_{011} mode while immersed in a uniform axial magnetic field. We treat analytically the linear problem of dependence of the axial velocity spread on the cavity length, and use simulation to examine non-linear aspects of the evolution of the spread with both the cavity length and the operating wavelength.

In a cavity operating in the TE_{011} mode, the electric field has only an azimuthal component with a radial distribution given by the first order Bessel function $J_1(k_c R)$, where k_c is the cutoff wave number, and R is the radial coordinate. For a single-energy electron beam with a sufficient small beam radius and only one guiding center at the origin, as shown in Fig. 1, the electrons with a larger gyration radius experience a stronger electric field decelerating force (for appropriate phase) than those with a smaller gyration radius. The larger the gyration radius is, the more energy the electron loses. By the coupling of energy with axial momentum (a relativistic effect), the axial velocity of the electron is increased if the effect of the time-dependent magnetic field is neglected. Therefore, as long as the beam pulse is sufficiently short the axial velocity spread will be improved.

For an actual electron beam, the guiding-center radius R_g ranges from zero to R_b, where R_b is the beam radius, and the gyration radius r_L ranges from zero to (R_b-R_g). In such a situation, we can consider the azimuthal field as the sum of infinite cyclotron harmonics. Of all these harmonics only the zeroth one is important. So for those electrons with non-zero guiding center, the previous analysis holds. From this we can see that the axial velocity spread of an electron beam with multi-guiding centers also can be improved.

Generally speaking, increasing the cavity length increases the interaction time. In this case, however, non-linear effects become important. As it is well known, when the cavity operating frequency is slightly greater than the electron relativistic cyclotron frequency, the electron beam effectively interacts with cyclotron harmonics and, as a result, resonant emission appears, which is the basis of the maser instability.[6] At this time, most of the electrons lie in the decelerating electric field of the fundamental harmonic because of the negative mass effect[7,8,9] which results in particle bunching in the azimuthal direction as explained by Sprangle and Drobot.[10] So once the beam is decelerated, no matter whether it experiences a net transverse acceleration or deceleration during the first-period interaction (depending on the phase of the pulsed beam entrance of the cavity), the decreased transverse velocities cannot go back to their original magnitude in the next interaction period.

Consequently, the axial velocity spread will continue to be reduced until another non-linear process (resonant absorption) arises, so that the transverse velocities of the electrons begin to increase, resulting in an increase in the axial velocity spread.

The beam conditioning presented here is different from the electron-beam cooling proposed by Hirshfield and Park.[11] In their proposal, the beam's distribution of energy is made narrower by use of both resonant emission and absorption. This process cannot be used to improve the axial velocity spread. For a single-energy electron beam with a spread in axial velocity, for example, it can do nothing because the width of the distribution in energy is null. The beam conditioner, in contrast, reduces the spread in axial velocity (instead of the energy spread) through the coupling of energy with axial momentum caused by resonant emission.

In Sec. II, a calculational model is set up to treat analytically a pulsed beam with the Vlasov theory. The perturbation distribution function of the pulsed beam conditioned by the RF cavity is derived and linear expressions for axial velocity spread are given. In Sec. III, numerical simulations are used to check the analytical results, and investigate the dependence of axial velocity spread on the cavity length and operating wavelength caused by the nonlinear interaction of the beam with the cavity field. Finally, in Sec. IV some conclusions are made.

II. Linear Kinetic Theory of the Beam Conditioner

In this section, based on linearized Vlasov equations, we will derive the perturbation distribution functions of a pulsed electron beam conditioned by the RF cavity and use them to obtain analytic expressions for the rms-normalized axial velocity spread.

In the model, we take the pulsed beam as a segment, which has a length L, of an infinitely long electron beam. We will first calculate the perturbation distribution function for the infinitely long beam, and then we use it to calculate the axial velocity spread of the considered segment. We assume that the electron beam is mono-energetic. The electron's transverse velocity is small compared with its axial velocity and variation in the pulse length is negligible when the pulsed beam goes from one end of the cavity to another. The beam pulse front is located at $z=0$ when $t=0$. At $t=d/v_0$ with d ($\geq L$) the cavity length and v_0 the total initial velocity, the beam pulse arrives at the front end of the cavity, and at $t=(d+L)/v_0$, the pulse beam has passed through the cavity, as shown in Fig. 2. For simplicity, the time-dependent magnetic field is neglected in the linear consideration.

The Vlasov equation describing the beam conditioner is given by

$$\frac{\partial f}{\partial t} + \mathbf{v}.\frac{\partial f}{\partial \mathbf{x}} + e\,(\mathbf{E} + \mathbf{v}\times\mathbf{B}).\frac{\partial f}{\partial \mathbf{p}} = 0\,, \tag{1}$$

where

$$\mathbf{E} = \hat{\varphi}\, E_0 J_1(k_c R)\sin\frac{\pi}{d}z\ \sin\omega t\ , \tag{2}$$

$$\mathbf{B} = \hat{z}\, B_0\ . \tag{3}$$

In Eqs. (2) and (3), the cylindrical coordinates are used, and $\hat{R}$, $\hat{\varphi}$ and $\hat{z}$ are all unit vectors; E_0 is the TE_{011}-mode electric field amplitude, B_0 is the applied uniform axial magnetic field, and ω is the cavity operating frequency. According to the small signal assumption $|E_0/B_0c|<<1$, where c is the light speed in free space, Eq. (1) can be linearized as

$$\left\{\frac{\partial}{\partial t}+\mathbf{v}.\frac{\partial}{\partial \mathbf{x}}+e\ (\mathbf{v}\times\mathbf{B}).\frac{\partial}{\partial \mathbf{p}}\right\}\begin{Bmatrix} f_0 \\ f_1^{(\mathrm{II})}\end{Bmatrix}=0\,, \tag{4}$$

and

$$\left\{\frac{\partial}{\partial t}+\mathbf{v}.\frac{\partial}{\partial \mathbf{x}}+e\ (\mathbf{v}\times\mathbf{B}).\frac{\partial}{\partial \mathbf{p}}\right\}f_1^{(\mathrm{I})}=-\,e\,\mathbf{E}.\frac{\partial f_0}{\partial \mathbf{p}}\,, \tag{5}$$

where f_0 is the equilibrium distribution function for both regions (I) and (II), and $f_1^{(\mathrm{I})}$ and $f_1^{(\mathrm{II})}$ are, respectively, the perturbation distribution functions for the two regions. In region (I), there is a cavity field, whereas in region (II) there is no cavity field. So $f_1^{(\mathrm{I})}$ satisfies Eq. (5) and $f_1^{(\mathrm{II})}$ satisfies Eq. (4).

At $t=0$ the electric field begins to condition the cavity-in part of the infinitely long electron beam so that it produces a perturbation of the distribution of the beam. Then the perturbation propagates with a velocity of v_z in the z-direction like a wave. So $f_1^{(\mathrm{I})}$ and $f_1^{(\mathrm{II})}$ are required to satisfy the following initial and boundary conditions

$$f_1^{(\mathrm{I})}(t\le 0)=f_1^{(\mathrm{II})}(t\le \tfrac{z-d}{v_z})=0\,, \tag{6}$$

$$f_1^{(\mathrm{I})}(z=d)=f_1^{(\mathrm{II})}(z=d)\,. \tag{7}$$

Eqs. (4)-(7) are the basis of finding perturbation functions. Only after obtaining them can we calculate the axial velocity spread.

A. Equilibrium Distribution Function

To calculate perturbation distribution functions we first have to determine the equilibrium distribution function from Eq. (4). According to the first order partial differential equation theory, any combination of constants of motion from characteristic equations of Eq. (4) is a solution. So, if we find the constants of motion we can use them to construct equilibrium distribution functions in terms of a given electron beam. For convenience, we use cylindrical coordinates in the momentum space just as in the configuration space, that is, $p_x=p_\perp\cos\phi$, $p_y=p_\perp\sin\phi$, and $p_z=p_z$.

Calculations indicate that the characteristic equations of Eq. (4) have six independent constants of motion:

$$C_1 = p_\perp \,, \tag{8}$$

$$C_2 = p_z \,, \tag{9}$$

$$C_3 = \phi - \frac{|e|B_0}{p_z} z \,, \tag{10}$$

$$C_4 = R\cos\varphi - \frac{p_\perp}{|e|B_0}\sin\phi \,, \tag{11}$$

$$C_5 = R\sin\varphi + \frac{p_\perp}{|e|B_0}\cos\phi \,, \tag{12}$$

$$C_6 = \phi - \Omega t \,, \tag{13}$$

where e is the electron charge, and $\Omega = |e|B_0/(\gamma m)$ is the relativistic cyclotron angular frequency, with $\gamma = \left(p_\perp^2 + p_z^2 + m^2c^2\right)^{1/2}/(mc)$ the relativistic factor and m the electron rest mass.

Because the electrons gyrate in the axial magnetic field, it is more convenient to use those constants of motion characterizing guiding centers to construct equilibrium distribution functions, for this gives us a clear physical picture.

Setting $r_L = p_\perp/|eB_0|$ and $\phi = \theta + (B_0/|B_0|)\pi/2$, from Eqs.(11) and (12) we have

$$R_g \cos\varphi_g = R\cos\varphi - r_L\cos\theta \,, \tag{14}$$

$$R_g \sin\varphi_g = R\sin\varphi - r_L\sin\theta \,, \tag{15}$$

where R_g and φ_g are radial and azimuthal coordinates of the guiding center and they are all constants of motion.

As shown in Fig. 3, when $B_0 > 0$, the electrons are right-rotated along the z-direction, and when $B_0 < 0$, the electrons are left-rotated. In the beam conditioner, unlike a gyrotron,[12,13] distinguishing the gyration direction is important because different gyration directions can result in different variations in velocity spread.

Suppose that the distribution of the guiding centers of the electron beam is uniform, so the equilibrium distribution function can be chosen as

$$f_0 = \delta(\gamma - \gamma_0)\,\mathrm{H}(p_\perp)\,\mathrm{H}[|eB_0|(R_b - R_g) - p_\perp]\,\mathrm{H}(R_g)\,\mathrm{H}(R_b - R_g)\,\mathrm{H}(p_z) \,, \tag{16}$$

where γ_0 is the initial relativistic factor, and H(x) is a unit step function. Since γ, $p_\perp$, p_z, and R_g are all constants of motion, f_0 given by Eq. (16) is a solution of Eq. (4).

B. Perturbation Distribution Function

We will use the method of integration along characteristics to solve for $f_1^{(I)}$ and then directly determine $f_1^{(II)}$ by using $f_1^{(I)}$ and arguments involving constants of motion.

The perturbation distribution function $f_1^{(I)}$ can be expressed as

$$f_1^{(I)} = -e \int_0^t \mathbf{E}' . \frac{\partial f_0}{\partial \mathbf{p}'} dt' . \tag{17}$$

To perform the above integration, we have to make local expansion of the electric field **E** in the guiding center (R_g, φ_g). Applying the Bessel function addition theorem

$$J_1(k_c R)\, e^{i(\varphi-\theta)} = \sum_{l=-\infty}^{+\infty} J_{1-l}(k_c R_g)\, e^{i(1-l)\varphi_g} J_l(k_c r_L)\, e^{i(l-1)\theta} , \tag{18}$$

we have

$$E_{r_L} = E_0 \sin\frac{\pi}{d} z \ \sin \omega t \sum_{l=-\infty}^{+\infty} (-1)^l J_l(k_c R_g) J_{l+1}(k_c r_L) \sin l(\varphi_g - \theta) , \tag{19}$$

$$E_\theta = E_0 \sin\frac{\pi}{d} z \ \sin \omega t \sum_{l=-\infty}^{+\infty} (-1)^l J_l(k_c R_g) J_{l+1}(k_c r_L) \cos l(\varphi_g - \theta) , \tag{20}$$

where E_{r_L} and E_θ are, respectively, the components of the r_L- and θ -directions in the guiding-center frame.

From Eqs. (19) and (20), we find that the electric field is expanded as a sum of infinite cyclotron harmonics. The amplitude of the l th harmonic is proportional to $J_l(k_c R_g)$. Because a small beam radius is used, $k_c R_g$ is much less than unity. In addition, because the field of the first harmonic varies azimuthally, its effect on an electron tends to cancel when the electron makes a revolution in the linear limit. So, the effect of the zeroth one is dominant. It should be noted that the zeroth harmonic has only an azimuthal component of the electric field and it is axisymmetric in the guiding-center frame, just like the whole TE_{011}-mode electric field in the waveguide-axial frame. In fact, if we let R_g approach zero, Eqs. (19) and (20) go back to Eq. (2).

The equations describing the characteristics are given by

$$z' = z - v_z (t - t') , \tag{21}$$

$$\theta' = \theta - \Omega (t - t') , \tag{22}$$

where $v_z = p_z/(\gamma m)$ is the axial velocity and it is also a constant of motion.

Substituting Eqs. (19)-(22) into Eq. (17), after a tedious calculation we can obtain the first-region perturbation distribution function

$$f_1^{(I)} = \sum_{l=-\infty}^{+\infty} -\frac{B_0}{|B_0|}\frac{1}{4} e E_0 F_l G_l^{(I)} , \tag{23}$$

where

$$F_l = (-1)^l \left\{ J_l(k_c R_g) J_{l+1}(k_c r_L) \left[\frac{\partial f_0}{\partial p_\perp} + \frac{p_\perp}{\gamma (mc)^2} \frac{\partial f_0}{\partial \gamma} \right] - \frac{1}{|eB_0|} J_{l+1}(k_c R_g) J_l(k_c r_L) \frac{\partial f_0}{\partial R_g} \right\} \tag{24}$$

$$\begin{aligned} G_l^{(I)} = & -\frac{1}{\omega_{1l}} \left\{ \sin\left[l\varphi_g + \left(\frac{\pi}{d} z - l\theta\right) + \omega t \right] - \sin\left[l\varphi_g + \left(\frac{\pi}{d} z - l\theta\right) - \left(\frac{\pi}{d} v_z - l\Omega\right) t \right] \right\} \\ & + \frac{1}{\omega_{2l}} \left\{ \sin\left[l\varphi_g - \left(\frac{\pi}{d} z + l\theta\right) - \omega t \right] - \sin\left[l\varphi_g - \left(\frac{\pi}{d} z + l\theta\right) + \left(\frac{\pi}{d} v_z + l\Omega\right) t \right] \right\} \\ & - \frac{1}{\omega_{3l}} \left\{ \sin\left[l\varphi_g + \left(\frac{\pi}{d} z - l\theta\right) - \omega t \right] - \sin\left[l\varphi_g + \left(\frac{\pi}{d} z - l\theta\right) - \left(\frac{\pi}{d} v_z - l\Omega\right) t \right] \right\} \\ & + \frac{1}{\omega_{4l}} \left\{ \sin\left[l\varphi_g - \left(\frac{\pi}{d} z + l\theta\right) + \omega t \right] - \sin\left[l\varphi_g - \left(\frac{\pi}{d} z + l\theta\right) + \left(\frac{\pi}{d} v_z + l\Omega\right) t \right] \right\} . \end{aligned} \tag{25}$$

In Eq. (25), ω_{1l}, ω_{2l}, ω_{3l}, and ω_{4l} are given by

$$\omega_{2l,1l} = \omega + \frac{\pi}{d} v_z \pm l\Omega , \tag{26}$$

$$\omega_{3l,4l} = \omega - \frac{\pi}{d} v_z \pm l\Omega . \tag{27}$$

On the basis of the perturbation distribution function in region (I), we can easily obtain the one in region (II). From Eq. (24) we can see that F_l is only a function of constants of motion and, of course, it is also a constant of motion. In Eq. (25), however, $G_l^{(I)}$ not only depends on the constants of motion φ_g, v_z, and Ω, but also depends on z, θ, and t, which are not constants of motion. So if we can use some constants of motion to take the place of them, then Eq. (4) is satisfied. To this end, setting $z = d$ in $G_l^{(I)}$ and then replacing t and θ by the following constants of motion:

$$t^* = t - \frac{1}{v_z}(z - d)\,, \tag{28}$$

$$\theta^* = \theta - \frac{\Omega}{v_z}(z - d)\,, \tag{29}$$

we obtain the second-region perturbation distribution function

$$f_1^{(II)} = \sum_{l=-\infty}^{+\infty} -\frac{B_0}{|B_0|}\frac{1}{4} e E_0 F_l G_l^{(II)}\,, \tag{30}$$

where

$$\begin{aligned} G_l^{(II)} = {} & \frac{H(t^*)}{\omega_{1l}}\left\{\sin\left[l(\varphi_g-\theta^*)+\omega t^*\right] - \sin\left[l(\varphi_g-\theta^*) - \left(\frac{\pi}{d}v_z - l\Omega\right)t^*\right]\right\} \\ & - \frac{H(t^*)}{\omega_{2l}}\left\{\sin\left[l(\varphi_g-\theta^*) - \omega t^*\right] - \sin\left[l(\varphi_g-\theta^*) + \left(\frac{\pi}{d}v_z + l\Omega\right)t^*\right]\right\} \\ & + \frac{H(t^*)}{\omega_{3l}}\left\{\sin\left[l(\varphi_g-\theta^*) - \omega t^*\right] - \sin\left[l(\varphi_g-\theta^*) - \left(\frac{\pi}{d}v_z - l\Omega\right)t^*\right]\right\} \\ & - \frac{H(t^*)}{\omega_{4l}}\left\{\sin\left[l(\varphi_g-\theta^*) + \omega t^*\right] - \sin\left[l(\varphi_g-\theta^*) + \left(\frac{\pi}{d}v_z + l\Omega\right)t^*\right]\right\}. \end{aligned} \tag{31}$$

Since t^* and θ^* are all constants of motion, $f_1^{(II)}$ satisfies the equilibrium Vlasov equation. Indeed, it is easy to verify that $f_1^{(I)}$ and $f_1^{(II)}$ satisfy the initial and boundary conditions.

C. Axial Velocity Spread

We have obtained perturbation functions and now we can use them to calculate the axial velocity spread.

The rms-normalized axial velocity spread is defined by

$$\sigma_{\beta_z} = \sqrt{\langle \beta_z^2 \rangle - \langle \beta_z \rangle^2}\,, \tag{32}$$

where β_z is the axial velocity normalized to the light speed c, the averages $\langle \beta_z \rangle$ and $\langle \beta_z^2 \rangle$ are given by

$$\langle \beta_z,\, \beta_z^2 \rangle = A \int (\beta_z,\, \beta_z^2)(f_0 + f_1)\, d^3\mathbf{p} d^3\mathbf{x}\,, \tag{33}$$

where f_1 denotes $f_1^{(I)}$ or $f_1^{(II)}$, and

$$A = \frac{1}{\int (f_0 + f_1)\, \mathrm{d}^3\mathbf{p}\mathrm{d}^3\mathbf{x}} . \tag{34}$$

From Eqs. (32) and (33), we have

$$\langle \beta_z^2 \rangle - \langle \beta_z \rangle^2 = \left[\langle \beta_z^2 \rangle_0 - \langle \beta_z \rangle_0^2\right] + \left[\langle \beta_z^2 \rangle_1 - \langle \beta_z \rangle_1^2\right] - 2 \langle \beta_z \rangle_0 \langle \beta_z \rangle_1 , \tag{35}$$

where $\langle\ \rangle_0$ and $\langle\ \rangle_1$ denote taking an average with f_0 and f_1 respectively.

Below we will calculate each term of the right-hand side in Eq. (35) and derive expressions for axial velocity spread when the front of the considered segment of beam arrives at $z=d$ and $z=d+L$, as shown in Fig. 2. The axial velocity spread of the segment at $z=d+L$ when $t=(d+L)/v_0$ is taken as the spread after the pulsed beam is conditioned by the cavity.

Using Eq. (16), we have

$$\langle \beta_z \rangle_0 = A \int \frac{p_z}{\gamma mc} f_0\, \mathrm{d}^3\mathbf{p}\mathrm{d}^3\mathbf{x} = \frac{1}{6} A\pi^2 L R_b^2 p_{\perp b}^2 mc , \tag{36}$$

where $p_{\perp b} = |eB_0|R_b$.

Similarly, we have

$$\langle \beta_z^2 \rangle_0 = \frac{1}{6} A\pi^2 \beta_0 L R_b^2 p_{\perp b}^2 mc\, \eta , \tag{37}$$

where

$$\eta = \frac{\beta_0^4}{\beta_{\perp b}^4}\left\{4\frac{\beta_{\perp b}^2}{\beta_0^2}\left(1-\frac{\beta_{zb}^3}{\beta_0^3}\right) - 3\frac{\beta_{\perp b}}{\beta_0}\left[\frac{\beta_{\perp b}}{\beta_0}\left(2\frac{\beta_{\perp b}^2}{\beta_0^2}-1\right)\frac{\beta_{zb}}{\beta_0} + \arcsin\frac{\beta_{\perp b}}{\beta_0}\right] + \frac{4}{5}\left[2-\left(2+3\frac{\beta_{\perp b}^2}{\beta_0^2}\right)\frac{\beta_{zb}^3}{\beta_0^3}\right]\right\} \tag{38}$$

with $\beta_0 = v_0/c$, $\beta_{\perp b} = p_{\perp b}/(\gamma_0 mc)$, and $\beta_{zb} = \left(\beta_0^2 - \beta_{\perp b}^2\right)^{1/2}$.

From Eqs. (23) and (30), we have

$$\langle \beta_z \rangle_1 = A \int \frac{p_z}{\gamma mc} f_1\, \mathrm{d}^3\mathbf{p}\mathrm{d}^3\mathbf{x}$$

$$= -\frac{B_0}{|B_0|}\frac{1}{4} Ae\, E_0 \sum_{l=-\infty}^{+\infty} \int \frac{p_z}{\gamma mc} F_l\, G_l\, \mathrm{d}^3\mathbf{p}\mathrm{d}^3\mathbf{x} , \tag{39}$$

where G_l denotes $G_l^{(\mathrm{I})}$ or $G_l^{(\mathrm{II})}$.

From Eqs. (14) and (15), making the change in integrated variables

$$R\,\mathrm{d}R\,\mathrm{d}\varphi = R_g\,\mathrm{d}R_g\,\mathrm{d}\varphi_g\,, \tag{40}$$

and inserting it into Eq.(39), we obtain

$$\langle\beta_z\rangle_1 = -\frac{B_0}{|B_0|}\,8\pi A d\,\frac{eE_0}{k_c c}\int_{-\infty}^{+\infty}\mathrm{d}p_z\int_0^{+\infty}p_\perp \mathrm{d}p_\perp\int_0^{+\infty}R_g\,\mathrm{d}R_g\,\frac{p_z}{\gamma mc}\,\Pi(t,\,v_z)$$
$$\times\left\{J_0(k_cR_g)\,J_1(k_cr_L)\left[\frac{\partial f_0}{\partial p_\perp}+\frac{p_\perp}{\gamma(mc)^2}\frac{\partial f_0}{\partial\gamma}\right]-\frac{1}{|eB_0|}J_1(k_cR_g)\,J_0(k_cr_L)\,\frac{\partial f_0}{\partial R_g}\right\},\tag{41}$$

where $\Pi(t,\,v_z)$ denotes $\Pi^{(\mathrm{I})}(t,\,v_z)$ or $\Pi^{(\mathrm{II})}(t,\,v_z)$. $\Pi^{(\mathrm{I})}(t,\,v_z)$ and $\Pi^{(\mathrm{II})}(t,\,v_z)$ are given by

$$\Pi^{(\mathrm{I})}(t,\,v_z) = \frac{\pi}{8d}\,k_c c\int_{d-L}^{d}G_0^{(\mathrm{I})}\,\mathrm{d}z$$
$$= \frac{1}{4}\,\frac{k_c c\,\omega}{\omega_+\omega_-}\left\{2\left[\cos\frac{\pi}{d}v_z t-\cos\frac{\pi}{d}(v_z t+L)-\cos\omega t\right]+\frac{\omega_+}{\omega}\cos\left(\omega t+\frac{L}{d}\pi\right)\right.$$
$$\left.+\frac{\omega_-}{\omega}\cos\left(\omega t-\frac{L}{d}\pi\right)\right\}\,, \tag{42}$$

$$\Pi^{(\mathrm{II})}(t,\,v_z) = \frac{\pi}{8d}\,k_c c\int_{d}^{d+L}G_0^{(\mathrm{II})}\,\mathrm{d}z$$
$$= \frac{1}{2}\,\frac{k_c c\,\omega}{\omega_+\omega_-}\left[1-\cos\left(\frac{\pi}{d}v_z t\right)-\left(\frac{\pi}{d}\frac{v_z}{\omega}\right)^2(1-\cos\omega t)\right]$$
$$\left(\frac{L}{v_z}>t\ge 0\right), \tag{43}$$

$$\Pi^{(\mathrm{II})}(t,\,v_z) = \frac{k_c c\,\omega}{\omega_+\omega_-}\left[\sin\frac{\pi L}{2d}\sin\left(\frac{\pi}{d}v_z t-\frac{\pi L}{2d}\right)-\left(\frac{\pi v_z}{d\,\omega}\right)^2\sin\frac{\omega L}{2v_z}\sin\left(\omega t-\frac{\omega L}{2v_z}\right)\right]$$
$$\left(t\ge\frac{L}{v_z}\right), \tag{44}$$

where $\omega_\pm = \omega\pm\pi v_z/d$.

Setting $v_z^* = (p_0^2 - p_\perp^2)^{1/2}/(\gamma_0 m)$ with p_0 the total initial electron's momentum, and expanding $\Pi(t,\,v_z^*)$ as a series in $p_\perp^2$, we have

$$\Pi(t,\,v_z^*) = D_0 + D_1 p_\perp^2 + D_2 p_\perp^4 + \cdots\,, \tag{45}$$

where $D_{0,1,2}$ denote $D_{0,1,2}^{(\mathrm{I})}$ or $D_{0,1,2}^{(\mathrm{II})}$. D_0, D_1, and D_2 are related by

$$D_1 = -\frac{\gamma_0}{2(mc)^2}\frac{\partial D_0}{\partial \gamma_0}, \tag{46}$$

$$D_2 = -\frac{1}{2(mc)^2}\left(D_1 + \frac{\gamma_0}{2}\frac{\partial D_1}{\partial \gamma_0}\right). \tag{47}$$

Making use of Eqs. (46) and (47) with small $\beta_{\perp b}$ taken into account, from Eq. (41) we obtain

$$\langle \beta_z \rangle_1 = -\frac{B_0}{|B_0|} 8\pi A d \frac{eE_0}{k_c c} mc S_{p_\perp}, \tag{48}$$

where

$$S_{p_\perp} = \frac{k_c R_b^2 p_{\perp b}^2}{|eB_0|}\left\{ \frac{1}{240}(D_0 - 2p_0^2 D_1)\beta_{\perp b}^2 - \frac{1}{3360}\frac{(\gamma_0 mc)^2 k_c^2}{|eB_0|^2}\beta_{\perp b}^4 \right.$$
$$\left. \times\left[(D_0 - 2p_0^2 D_1) - 5\frac{|eB_0|^2}{k_c^2}(3D_1 - 4p_0^2 D_2)\right]\right\}. \tag{49}$$

In a similar way, we can obtain

$$\langle \beta_z^2 \rangle_1 = -\frac{B_0}{|B_0|} 8\pi A d \frac{eE_0}{k_c c} mc T_{p_\perp}, \tag{50}$$

where

$$T_{p_\perp} = \frac{k_c R_b^2 p_{\perp b}^2}{|eB_0|}\left\{ \frac{1}{120}\beta_0(D_0 - p_0^2 D_1)\beta_{\perp b}^2 - \frac{1}{3360}\frac{\beta_{\perp b}^4}{\beta_0}\left[\frac{2p_0^2 k_c^2}{|eB_0|^2}(D_0 - p_0^2 D_1)\right.\right.$$
$$\left.\left. + 5[(D_0 - p_0^2 D_1) - 4p_0^2(D_1 - p_0^2 D_2)]\right]\right\}. \tag{51}$$

The normalized coefficient A in Eqs. (48) and (50) can be found from Eq. (34) and it is given by

$$A = \frac{6}{\pi^2 L R_b^2 p_{\perp b}^2 mc}\frac{\beta_0}{(A_0 + A_1)}, \tag{52}$$

where

$$A_0 = 1 - \frac{1}{10}\frac{\beta_{\perp b}^2}{\beta_0^2} - \frac{47}{2800}\frac{\beta_{\perp b}^4}{\beta_0^4}, \tag{53}$$

$$A_1 = -a\beta_{\perp b}^2 + \left(\frac{a}{5\beta_0^2} - b\right)\beta_{\perp b}^4, \tag{54}$$

with

$$a = -\frac{2}{5\pi}\frac{d}{L}\frac{E_0}{B_0 c}p_0^2 D_1, \tag{55}$$

$$b = \frac{1}{35\pi}\frac{d}{L}\frac{E_0}{B_0 c}\frac{(\gamma_0 mc)^2 k_c^2}{|eB_0|^2}p_0^2 D_1 . \tag{56}$$

Inserting Eq. (52) into Eq. (48), keeping them up to the order of $\beta_{\perp b}^4$, and only taking those terms of the first order of $E_0/(B_0 c)$, we obtain

$$\langle\beta_z\rangle_1 = \frac{1}{\pi}\frac{E_0}{B_0 c}\frac{d}{L}\left\{\frac{1}{5}\beta_0(D_0 - 2p_0^2 D_1)\beta_{\perp b}^2 + \frac{1}{\beta_0}\left[\frac{1}{14}p_0^2(3D_1 - 4p_0^2 D_2)\right.\right.$$
$$\left.\left. - \left(\frac{1}{50} + \frac{1}{70}\frac{k_c^2 p_0^2}{|eB_0|^2}\right)(D_0 - 2p_0^2 D_1)\right]\beta_{\perp b}^4\right\} . \tag{57}$$

Similarly, we have

$$\langle\beta_z^2\rangle_1 = \frac{1}{\pi}\frac{E_0}{B_0 c}\frac{d}{L}\left\{\frac{2}{5}\beta_0^2(D_0 - p_0^2 D_1)\beta_{\perp b}^2 + \left[\frac{2}{7}p_0^2(D_1 - p_0^2 D_2)\right.\right.$$
$$\left.\left. - \left(\frac{39}{350} + \frac{1}{35}\frac{k_c^2 p_0^2}{|eB_0|^2}\right)(D_0 - p_0^2 D_1)\right]\beta_{\perp b}^4\right\} . \tag{58}$$

Substituting Eq. (52) into Eqs. (36) and (37), and subtracting the square of Eq. (36) from Eq. (37), we obtain

$$\langle\beta_z^2\rangle_0 - \langle\beta_z\rangle_0^2 = \frac{11}{1400}\frac{\beta_{\perp b}^4}{\beta_0^2} + \frac{1}{\pi}\frac{E_0}{B_0 c}\frac{d}{L}\left\{-\frac{2}{5}\beta_0^2 p_0^2 D_1\beta_{\perp b}^2 + \left[\frac{1}{14}p_0^2(D_1 - 4p_0^2 D_2)\right.\right.$$
$$\left.\left. + \left(\frac{3}{25} + \frac{1}{35}\frac{k_c^2 p_0^2}{|eB_0|^2}\right)p_0^2 D_1\right]\beta_{\perp b}^4\right\} . \tag{59}$$

Using Eqs. (36), (52), and (57), we have

$$-2\langle\beta_z\rangle_0\langle\beta_z\rangle_1 = \frac{1}{\pi}\frac{E_0}{B_0 c}\frac{d}{L}\left\{ -\frac{2}{5}\beta_0^2(D_0 - 2p_0^2 D_1)\beta_{\perp b}^2 - \left[\frac{1}{7}p_0^2(3D_1 - 4p_0^2 D_2)\right.\right.$$

$$\left.\left. -\left(\frac{2}{25} + \frac{1}{35}\frac{k_c^2 p_0^2}{|eB_0|^2}\right)(D_0 - 2p_0^2 D_1)\right]\beta_{\perp b}^4\right\} . \qquad (60)$$

Substituting Eqs. (58), (59), and (60) into Eq. (35), and neglecting $\langle\beta_z\rangle_1^2$ because it is proportional to $(E_0/B_0c)^2$, we obtain

$$\langle\beta_z^2\rangle - \langle\beta_z\rangle^2 = \frac{11}{1400}\frac{\beta_{\perp b}^4}{\beta_0^2} - \frac{11}{350\pi}\frac{E_0}{B_0 c}\frac{d}{L}\beta_{\perp b}^4 D_0 . \qquad (61)$$

D_0 in the above can be found from Eqs. (42)-(45), and they are given by

$$D_0^{(\mathrm{I})} = \frac{1}{4}\frac{k_c c\,\omega}{\omega^2 - \left(\frac{\pi}{d}v_0\right)^2}\left\{ 2\left[\cos\frac{\pi}{d}v_0 t - \cos\frac{\pi}{d}(v_0 t + L) - \cos\omega t\right]\right.$$

$$\left. + \left(1 + \frac{\pi v_0}{d\omega}\right)\cos\left(\omega t + \frac{\pi}{d}L\right) + \left(1 - \frac{\pi v_0}{d\omega}\right)\cos\left(\omega t - \frac{\pi}{d}L\right)\right\} , \qquad (62)$$

$$D_0^{(\mathrm{II})} = \frac{1}{2}\frac{k_c c\,\omega}{\omega^2 - \left(\frac{\pi}{d}v_0\right)^2}\left[1 - \cos\frac{\pi}{d}v_0 t - \left(\frac{\pi v_0}{d\omega}\right)^2(1 - \cos\omega t)\right]$$

$$\left(\frac{L}{v_0} > t \geq 0\right), \qquad (63)$$

$$D_0^{(\mathrm{II})} = \frac{k_c c\,\omega}{\omega^2 - \left(\frac{\pi}{d}v_0\right)^2}\left[\sin\frac{\pi L}{2d}\sin\frac{\pi}{d}\left(v_0 t - \frac{\pi L}{2d}\right) - \left(\frac{\pi v_0}{d\omega}\right)^2\sin\frac{\omega L}{2v_0}\sin\left(\omega t - \frac{\omega L}{2v_0}\right)\right]$$

$$\left(t \geq \frac{L}{v_0}\right). \qquad (64)$$

From Eqs. (62)-(64) we can see that the velocity spread of the segments of beam at $z=d$ and $z=d+L$ are dependent on time; but only the spread of the segment, located at $z=d+L$, at $t=(d+L)/v_0$ is the one we need. If L is infinitely short, however, the two segments should have the same spread.

Setting $t=d/v_0$ in Eq. (62) and $t=(d+L)/v_0$ in Eq. (64), and then inserting them into Eq. (61), respectively, we obtain the expressions for rms-normalized axial velocity spread

$$\sigma_{\beta_z}^{(I)} = \sqrt{\frac{11}{1400}}\,\frac{1}{\beta_0}\left(\frac{R_b e B_0}{\gamma_0 mc}\right)^2 \left\{ 1 + \frac{4}{\pi}\frac{E_0}{B_0 c}\beta_0^2 \frac{d}{L}\,\frac{\sqrt{1-\left(\frac{\lambda}{2d}\right)^2}}{1-\left(\frac{\beta_0\lambda}{2d}\right)^2} \right.$$

$$\left. \times\left[2\sin^2\left(\frac{\pi L}{2d}\right)\cos^2\left(\frac{\pi d}{\beta_0\lambda}\right) + \frac{\beta_0\lambda}{4d}\sin\frac{\pi L}{d}\sin\frac{2\pi d}{\beta_0\lambda}\right] \right\}^{\frac{1}{2}}, \qquad (65)$$

$$\sigma_{\beta_z}^{(II)} = \sqrt{\frac{11}{1400}}\,\frac{1}{\beta_0}\left(\frac{R_b e B_0}{\gamma_0 mc}\right)^2 \left\{ 1 + \frac{4}{\pi}\frac{E_0}{B_0 c}\beta_0^2 \frac{d}{L}\,\frac{\sqrt{1-\left(\frac{\lambda}{2d}\right)^2}}{1-\left(\frac{\beta_0\lambda}{2d}\right)^2} \right.$$

$$\left. \times\left[\sin^2\left(\frac{\pi L}{2d}\right) + \left(\frac{\beta_0\lambda}{2d}\right)^2 \sin\frac{\pi L}{\beta_0\lambda}\sin\frac{\pi(2d+L)}{\beta_0\lambda}\right] \right\}^{\frac{1}{2}}, \qquad (66)$$

where λ is the cavity operating wavelength.

Eq. (65) describes the axial velocity spread when the pulsed beam arrives at the front of the cavity and Eq. (66) describes the spread when it leaves the cavity. When the beam length approaches zero, the two formulas give the same result, as expected. Because the linear modification of the axial velocity spread is caused by the zeroth harmonic, it only depends on the cavity length normalized to an operating wavelength; that is, there is no dependence on what wavelength is used.

Taking E_0=7.5x10^4 Volt/cm, B_0=2500 Gauss, (E_0/B_0c=0.1), R_b=1 cm and γ_0=2.47, from Eq. (66) we have drawn the dependence of the rms-normalized axial velocity spread on the normalized cavity length. As shown in Fig. 4, we can see that the maximum of the spread increases with the pulse length. For the pulsed beam with a length of 0.01 wavelength, the velocity spread is maximumly improved when the normalized cavity length is about 0.62. For the pulsed beam with a length of 0.5 wavelength, however, the spread is not improved and instead it is deteriorated. From this it can be inferred that the effect of the pulse length on velocity spread is important. From Fig. 4, we also can find that the spread varies quasi-periodically with the cavity length. The varying amplitude approaches zero as the cavity length increases infinitely. According to Eq. (66), the quasi-periodicity of the dependence of the spread on the cavity length is related to the electron's initial energy, the operating wavelength, and the pulse length.

It should be noted that the spread for 0.5 normalized cavity length, about 3.41%, is the same as that of the equilibrium beam. It seems that the beam is not affected at all when it passes through the cavity. This can be explained as follows: when the cavity length is equal to half an operating wavelength, the waveguide radius appproaches infinity and so the electric field within the electron beam vanishes. Accordingly, the beam cannot be conditioned.

The linear theory indicates that the improvement on the spread is very small. Therefore, investigation of non-linear processes for the beam conditioner is necessary.

III. Nonlinear Evaluation of the Beam Conditioner

In this section we will use the basic equations governing the nonlinear behavior of the beam conditioner to examine relations between the axial velocity spread and the cavity length.

In our procedure, the vacuum-cavity TE_{011}-mode fields are used and the contribution of the pulsed beam to the cavity fields is neglected. This is quite reasonable because the transverse velocities of the beam are rather small in the beam conditioner, unlike the cyclotron maser where an electromagnetic wave is efficiently amplified through the coupling between the wave and an electron beam with much larger averaged transverse velocity.[10] The electron orbits are related to the fields through the relativistic Lorentz force equations in the single-particle simulation. First, in order to check the previous linear kinetic theory we use only the TE_{011}-mode electric field and neglect its magnetic field to compute a single pulsed beam. Then we use both the electric and magnetic fields of the TE_{011} mode to compute the same pulsed beam and compare them with each other. This simulation reveals the nonlinear evolution of the rms-normalized axial velocity spread as a function of cavity length.

When only the electric field is used in the simulation, the axial momentum is a constant and it is examined to check the validity of the calculation. In the general case, all three checks have been passed by the code. When both the electric and magnetic fields are included, we use Liouville's theorem to check the code by computing the Jacobi determinant (time is taken as an independent variable) and, also, by reversing the computation and using the final values of a particle as initial conditions.

A. Lorentz Force Equations in the Guiding Center

In the previous linear theory, for the convenience of calculation, the TE_{011}-mode field is expanded as a sum of infinite harmonics. In the computation, however, it is more convenient to resove directly the TE_{011}-mode field into components in the guiding-center frame without expansion into harmonics.

In the waveguide-axial frame, the TE_{011}-mode fields are given by

$$E_\varphi = E_0 J_1(k_c R) \sin \frac{\pi}{d} z \sin \omega t \ , \tag{67}$$

$$B_R = - E_0 \frac{1}{\omega} \frac{\pi}{d} J_1(k_c R) \cos \frac{\pi}{d} z \cos \omega t \ , \tag{68}$$

$$B_z = - E_0 \frac{k_c}{\omega} J_0(k_c R) \sin \frac{\pi}{d} z \cos \omega t \ . \tag{69}$$

In the guiding-center frame, E_φ and B_R are resolved into the following:

$$E_{r_L} = E_0 J_1(k_c R) \frac{R_g}{R} \sin\left(\theta - \varphi_g\right) \sin \frac{\pi}{d} z \sin \omega t \ , \tag{70}$$

$$E_\theta = E_0 J_1(k_c R) \left[\frac{R_g}{R} \cos\left(\theta - \varphi_g\right) + \frac{r_L}{R}\right] \sin \frac{\pi}{d} z \sin \omega t \ , \tag{71}$$

$$B_{r_L} = - E_0 \frac{1}{\omega} \frac{\pi}{d} J_1(k_c R) \left[\frac{R_g}{R} \cos\left(\theta - \varphi_g\right) + \frac{r_L}{R} \right] \cos \frac{\pi}{d} z \cos \omega t \ , \tag{72}$$

$$B_\theta = E_0 \frac{1}{\omega} \frac{\pi}{d} J_1(k_c R) \frac{R_g}{R} \sin\left(\theta - \varphi_g\right) \cos \frac{\pi}{d} z \cos \omega t \ , \tag{73}$$

where

$$R = \sqrt{R_g^2 + r_L^2 + 2 R_g r_L \cos\left(\theta - \varphi_g\right)} \ . \tag{74}$$

Here we use the same symbols as those in the linear theory. But it should be noted that some of them have different mathematical contents. For example, in the kinetic theory R_g and φ_g are functions of both the momentum variables and the configuration variables, whereas in this single-particle simulation they are fixed for a given guiding-center frame.

From Eqs. (70)-(73), the Lorentz force equations in the guiding-center frame can be written as

$$\frac{d\bar{r}}{d\bar{z}} = \frac{\pi}{\bar{R}_b} \sqrt{4\bar{d}^2 - 1} \frac{\beta_1}{\beta_3} \ , \tag{75}$$

$$\frac{d\bar{\theta}}{d\bar{z}} = \frac{1}{2\bar{R}_b} \sqrt{4\bar{d}^2 - 1} \frac{1}{\bar{r}} \frac{\beta_2}{\beta_3} \ , \tag{76}$$

$$\frac{d\bar{t}}{d\bar{z}} = \frac{\bar{d}}{\beta_3} \ , \tag{77}$$

$$\frac{d\beta_1}{d\bar{z}} = \pi \sqrt{4\bar{d}^2 - 1} \frac{1}{\beta_3} \left\{ \frac{\beta_2^2}{\bar{R}_b \bar{r}} - \frac{1}{\gamma} \left[\left(1 - \beta_1^2\right) \bar{E}_r - \beta_1 \beta_2 \bar{E}_\theta - \beta_3 \bar{B}_\theta + \beta_2 \bar{B}_z \right] \right\} , \tag{78}$$

$$\frac{d\beta_2}{d\bar{z}} = \pi \sqrt{4\bar{d}^2 - 1} \frac{1}{\beta_3} \left\{ - \frac{\beta_1 \beta_2}{\bar{R}_b \bar{r}} + \frac{1}{\gamma} \left[\beta_1 \beta_2 \bar{E}_r - \left(1 - \beta_2^2\right) \bar{E}_\theta - \beta_3 \bar{B}_r + \beta_1 \bar{B}_z \right] \right\} , \tag{79}$$

$$\frac{d\beta_3}{d\bar{z}} = \pi \sqrt{4\bar{d}^2 - 1} \frac{1}{\beta_3} \frac{1}{\gamma} \left[\beta_1 \beta_3 \bar{E}_r + \beta_2 \beta_3 \bar{E}_\theta + \beta_2 \bar{B}_r - \beta_1 \bar{B}_\theta \right] , \tag{80}$$

where

$$\bar{E}_r = \alpha_1 \left[J_0(\bar{R}_b \bar{R}) + J_2(\bar{R}_b \bar{R}) \right] \bar{R}_g \sin 2\pi\left(\bar{\theta} - \bar{\varphi}_g\right) \sin \pi \bar{z} \sin 2\pi \bar{t} \ , \tag{81}$$

$$\bar{E}_\theta = \alpha_1[J_0(\bar{R}_b\bar{R})+J_2(\bar{R}_b\bar{R})]\left[\bar{R}_g\cos 2\pi\left(\bar{\theta}-\bar{\varphi}_g\right)+\bar{r}\right]\sin\pi\bar{z}\sin 2\pi\bar{t}\ , \quad (82)$$

$$\bar{B}_r = -\ \alpha_2[J_0(\bar{R}_b\bar{R})+J_2(\bar{R}_b\bar{R})]\left[\bar{R}_g\cos 2\pi\left(\bar{\theta}-\bar{\varphi}_g\right)+\bar{r}\right]\cos\pi\bar{z}\cos 2\pi\bar{t}, \quad (83)$$

$$\bar{B}_\theta = \alpha_2[J_0(\bar{R}_b\bar{R})+J_2(\bar{R}_b\bar{R})]\bar{R}_g\sin 2\pi\left(\bar{\theta}-\bar{\varphi}_g\right)\cos\pi\bar{z}\cos 2\pi\bar{t}, \quad (84)$$

$$\bar{B}_z = \alpha_3 - \alpha_4 J_0(\bar{R}_b\bar{R})\sin\pi\bar{z}\cos 2\pi\bar{t}\ , \quad (85)$$

with $\alpha_1=|e|R_bE_0/(2mc^2)$, $\alpha_2=|e|R_bE_0/(4\bar{d}mc^2)$, $\alpha_3=|e|B_0/(mk_cc)$, and $\alpha_4=|e|E_0/(m\omega c)$. The normalized quantities appearing in Eqs. (75)-(85) are defined by $\bar{z}=z/d$, $\bar{r}=r_L/R_b$, $\bar{\theta}=\theta/(2\pi)$, $\bar{t}=\omega t/(2\pi)$, $\beta_1=(dr_L/dt)/c$, $\beta_2=(r_L d\theta/dt)/c$, $\beta_3=(dz/dt)/c$, $\bar{d}=d/\lambda$, $\bar{R}_b=k_cR_b$, $\bar{R}_g=R_g/R_b$, $\bar{\varphi}_g=\varphi_g/(2\pi)$, $\bar{R}=R/R_b$, and $\gamma=(1-\beta_1^2-\beta_2^2-\beta_3^2)^{-1/2}$.

B. Simulation Results

We used Eqs. (75)-(80) and made computations for a pulsed beam, immersed in a 2500 Gauss axial magnetic field, with a length of 0.5 cm, a radius of 1 cm, and an initial relativistic factor of 2.47.[14] The initial electron's relativistic cyclotron frequency is 2.83 GHz, corresponding to its relativistic cyclotron wavelength 10.6 cm in free space. Three layers of sample electrons are taken within the beam and each layer has six guiding centers with 209 electrons. Because the TE_{011}-mode fields are axisymmetrical, the six guiding centers are all placed at $\varphi_g=0$. The guiding centers are distributed uniformly along the radial direction with the coordinates R_g/R_b = 0.0, 0.2, 0.4, 0.6, 0.8, and 1.0, and the distribution of the electrons on gyration orbits simulates the equilibrium distribution function, given by Eq. (16), of neglecting the gradient effect of the guiding center. The amplitude of the cavity electric field is taken as 7.5×10^4 Volt/cm.

First, let us examine the numerical simulation using only the electric field. Taking the operating wavelength as 10 cm, and the entrance time of the pulsed beam front as zero and 0.5T (T is the period of the cavity field), we find that the linear results agree qualitatively with the ones from the simulation, as shown in Fig. 5 and Fig. 6, respectively. Both in the linear and simulation results, the axial velocity spread oscillates with the cavity length and the oscillation damps gradually. When the cavity length is larger than one wavelength, however, the nonlinear effect becomes very considerable. In the nonlinear interaction, the mean value of oscillation of the velocity spread evidently reduces with the cavity length, whereas in the linear result it keeps constant. Since the reduction in the mean value of oscillation is caused by resonant emission, it should not depend on the phase at which the pulsed beam enters the cavity. Figure 7 shows the dependence of the axial velocity spread on the normalized cavity length for three different entrance phases. From Fig. 7 we can see, indeed, that these mean values are almost the same.

As we mentioned previously, when an electron loses energy, its axial velocity increases, and the smaller the axial velocity is, the more it increases. Accordingly, the beam's axial velocity spread is improved. The simulation confirms the above statement. In the linear regime (the normalized cavity length is less than unity), the velocity spread is decreased when the averaged normalized energy (the averaged

relativistic factor) is less than its initial value, and it is increased when the averaged energy is larger than its initial value, as shown in Fig. 8. In the nonlinear regime, the mean value of oscillation of the averaged energy goes down continuously and the mean value of the velocity spread is decreased gradually. The dependence of the averaged normalized axial velocity on the normalized cavity length is shown in Fig. 9.

Then we made simulations for the same pulsed beam with the whole TE_{011}-mode field, including both electric and magnetic fields. The results are shown in Fig. 10a, Fig. 11, and Fig. 12. Comparing Fig. 10a with Fig. 7, however, we find that there are two main differences. In the linear regime, the effect of the time-dependent magnetic field is so important that the velocity spread dependence on the cavity length is contrary to that without the time-dependent magnetic field taken into account. In the nonlinear regime, the mean value of the axial velocity spread is more rapidly decreased (also see Fig. 14). The dependence of the rms-normalized energy spread on the normalized cavity length is shown in Fig. 10b. From Fig. 10a and Fig. 10b we find that for short cavities no matter whether the axial velocity spread is increased or decreased, the energy spread is always increased.

To examine the dependence of the axial velocity spread on the operating wavelength and to find out at what wavelength the beam conditioner can best improve the beam's axial velocity spread, we made simulations for different wavelengths. The result indicates that the axial velocity spread strongly depends on the operating wavelength, as shown in Fig. 13. For a wavelength of 11 cm (2.73 GHz), the mean value of the axial velocity spread reduces most rapidly with the normalized cavity length. For too long, or short, a wavelength compared with 10.6 cm (corresponding to the initial electron's relativistic cyclotron frequency 2.83 GHz), the axial velocity spread cannot be improved. From Fig. 13, we also can find that in the linear regime the dependences of axial velocity spread on the cavity length normalized to different wavelengths are almost the same, which means that there is little dependence on what wavelength is used to normalize the cavity length. From this we can deduce that the effect of the zeroth harmonic is dominant and the effect of the first harmonic is negligible in the linear regime, which agrees with the previous linear theory.

We know that the resonant radiation appears only at the operating frequency slightly greater than the electron's relativistic cyclotron frequency. Now the relativistic cyclotron frequency is 2.83 GHz (10.6 cm). Why can the pulsed beam generate resonant radiation at the frequencies less than 2.83 GHz? This is because the beam has an axial velocity spread and the axial velocity spread Doppler-widens the frequency range of resonant radiation. In addition, in a cavity the beam can also effectively interact with the backward wave.

Although the axial velocity spread rapidly reduces with the cavity length when the cavity operates at a wavelength of 11 cm, it very soon reaches its minimum value of 3.9%, only decreased by 2.1% compared with its initial value of 6%. If the cavity operates at 10 cm, the axial velocity spread decreases down to 1.8%, less than one third of its initial value. However, the cavity length is greater than that for the 11 cm case, as shown in Fig. 14.

IV. Conclusions

We have developed a linear kinetic theory to investigate a conditioner for a helically transported electron beam. The expressions for axial velocity spread of a pulsed beam conditioned by the RF cavity operating in TE_{011}-mode were derived. Numerical simulations were used to check the linear theory and it was found that

the linear results are qualitatively in agreement with those from the simulations. We also have examined the nonlinear evolution of the axial velocity spread with the cavity length and the cavity operating wavelength due to the negative mass effect. In summary, we can make the following conclusions. In the linear regime, in which the cavity length is less than one operating wavelength, the modification of axial velocity spread is caused mainly by the interaction of the electrons with the zeroth harmonic, and hence whether the axial velocity spread is improved and this improvement mainly depends on the phase at which the pulsed beam enters the cavity and only slightly depends on the operating wavelength. In the nonlinear regime, the variation in axial velocity spread results from the interaction of the electrons with the fundamental harmonic based on the negative mass effect, and so it strongly depends on the operating wavelength and only slightly depends on the entrance phase of the pulsed beam. The simulation for a pulsed beam with a length of 0.5 cm, passing through a cavity operating at a wavelength of 10 cm, indicates that the rms-normalized axial velocity spread can be reduced down to 1.8%, less than one third of its initial value. From this we see that a beam conditioner can be used to decrease the spread in axial velocities for a low-energy electron beam.

Acknowledgments

The idea was proposed by Andrew M. Sessler, to whom the author is indebted for his many good comments on this paper. The author also wishes to thank Li-Hua Yu of BNL and Ming Xie of LBL for their helpful discussions.

References

1. A. M. Sessler, D. Whittum, and Li-Hua Yu, Phys.Rev.Lett. 68, 309 (1992).
2. A. M. Sessler, Lawrence Berkeley Laboratory ESG Tech Note 190, Mar. 10, 1992.
3. Li-Hua Yu, A. M. Sessler, and D. H. Whittum, Lawrence Berkeley Laboratory Report No. LBL-31198, 1991.
4. Y. H. Chin, K. J. Kim, and M. Xie, Lawrence Berkeley Laboratory Report No. LBL-30673, 1991.
5. K. -J. Kim, Lawrence Berkeley Laboratory Report No. LBL-31925, 1992.
6. J. L. Hirshfield and J. M. Wachtel, Phys. Rev. Lett. 12, 553 (1964).
7. C. E. Nielsen, A. M. Sessler, and K. R. Symon, in Proceedings of the International Conference on Accelerators (CERN, Geneva, 1959), p. 239.
8. V. K. Neil and W. Heckrotte, J. Appl. Phys. 36, 2761 (1965).
9. Y. Y. Lau and R. J. Briggs, Phys. Fluids 14, 967 (1971).
10. P. Sprangle and A. T. Drobot, IEEE MTT-25, 528 (1977).
11. J. L. Hirshfield and G. S. Park, Phys. Rev. Lett. 66, 2312 (1991); 68, 134 (1992).
12. K. R. Chu, Phys. Fluids 21, 2354 (1978).
13. Liu Shenggang, Scientia Sinica XXII, 901 (1979).
14. M. E. Conde and G. Bekefi, Phys. Rev. Lett. 67, 3082 (1991).

Figure Captions

Fig. 1. Distribution of the amplitude of the TE_{011}-mode electric field along the radial direction and electrons rotating around the waveguide axis.

Fig. 2. Calculational model. The pulsed electron beam is taken as a segment of an infinitely long beam. When $t=0$, the front of the segment of beam is located at $z=0$. When $t=d/v_0$ and $t=(d+L)/v_0$, the front is at $z=d$ and $z=(d+L)$, respectively.

Fig. 3a. The guiding-center frame when the applied uniform magnetic field is directed in the positive z-direction.

Fig. 3b. The guiding-center frame when the applied uniform magnetic field is directed in the negative z-direction.

Fig. 4. Dependence of the rms-normalized axial velocity spread on the normalized cavity length. The entrance time of the pulsed beams is zero.

Fig. 5. Comparison of the linear result with that from the simulation using only the electric field. The operating wavelength is 10 cm and the entrance time is zero. When the normalized cavity length is equal to unity, the axial velocity spread is increased.

Fig. 6. Comparison of the linear result with that from the simulation of using only the electric field. The operating wavelength is 10 cm and the entrance time is 0.5 T. When the normalized cavity length is equal to unity, the axial velocity spread is decreasd.

Fig. 7. Dependence of the rms-normalized axial velocity spread on the normalized cavity length when the pulsed beam enters the cavity at different times. Only the electric field is included and the operating wavelength is 10 cm.

Fig. 8. Dependence of the rms-normalized axial velocity spread and the averaged normalized energy on the normalized cavity length. Only the electric field is included and the operating wavelength is 10 cm. The entrance time is zero.

Fig. 9. Dependence of the averaged normalized axial velocity and the rms-normalized axial velocity spread on the normalized cavity length. Only the electric field is included and the operating wavelength is 10 cm. The entrance time is zero.

Fig. 10a. Dependence of the rms-normalized axial velocity spread on the normalized cavity length when the pulsed beam enters the cavity at different times. Both the electric and the magnetic fields are included and the operating wavelength is 10 cm.

Fig. 10b. Dependence of the rms-normalized energy spread on the normalized cavity length. The parameters are the same as those in Fig. 10a.

Fig. 11. Dependence of the rms-normalized axial velocity spread and the averaged normalized energy on the normalized cavity length. Both the electric and magnetic fields are included and the operating wavelength is 10 cm. The entrance time is zero.

Fig. 12. Dependence of the averaged normalized axial velocity and the rms-normalized axial velocity spread on the normalized cavity length. Both the electric and magnetic fields are included and the operating wavelength is 10 cm. The entrance time is zero.

Fig. 13. Dependence of the rms-normalized axial velocity spread on the cavity length normalized to different operating wavelengths. Both the electric and magnetic fields are included and the entrance time is zero. In the linear regime, the dependences are almost the same.

Fig. 14. Optimization of the operating wavelength (the entrance time is zero). When the operating wavelength is 10 cm, a little less than the initial electron's relativistic cyclotron wavelength, the beam conditioner best improves the axial velocity spread.

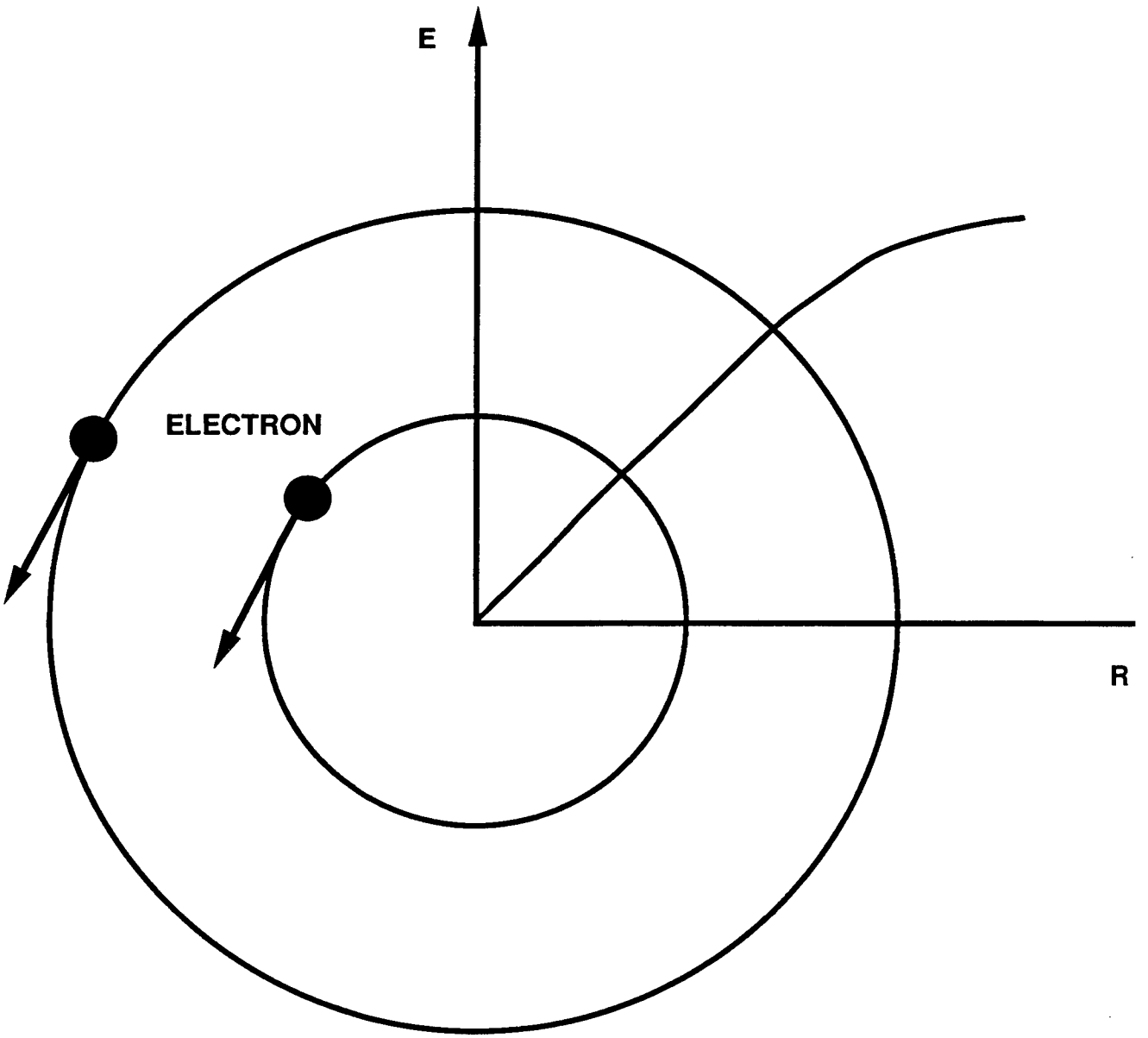

Fig.1

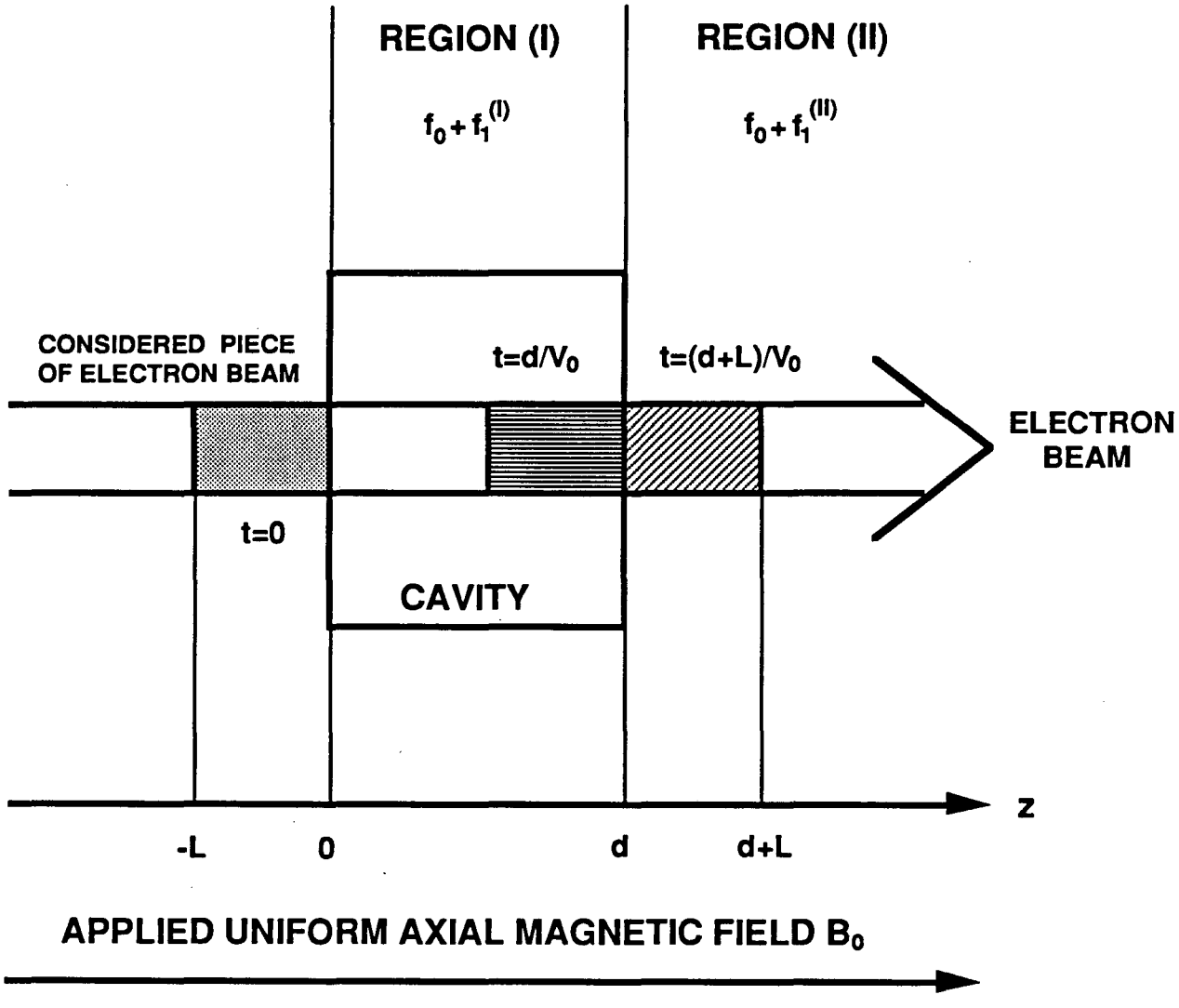
REGION (I)
REGION (II)
$f_0 + f_1^{(I)}$
$f_0 + f_1^{(II)}$
CONSIDERED PIECE OF ELECTRON BEAM
t=d/V0
t=(d+L)/V0
ELECTRON BEAM
t=0
CAVITY
z
-L
0
d
d+L
APPLIED UNIFORM AXIAL MAGNETIC FIELD B0

Fig.2

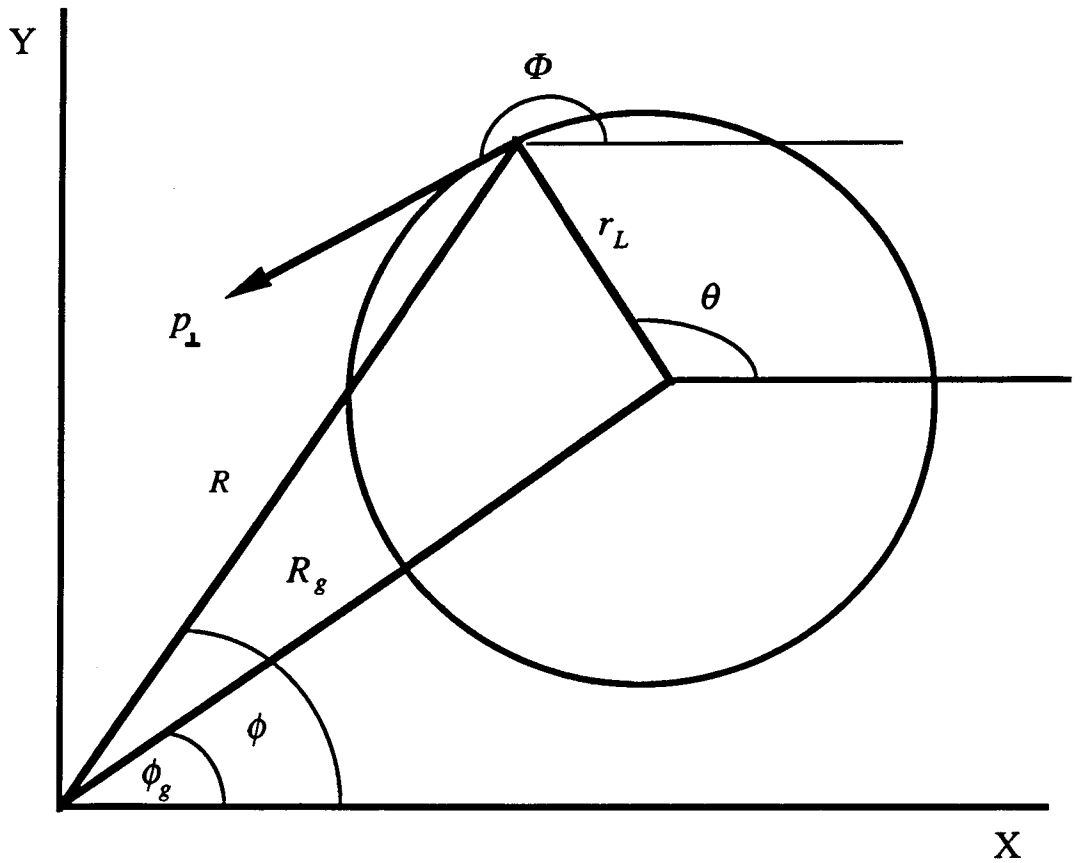

Fig.3a

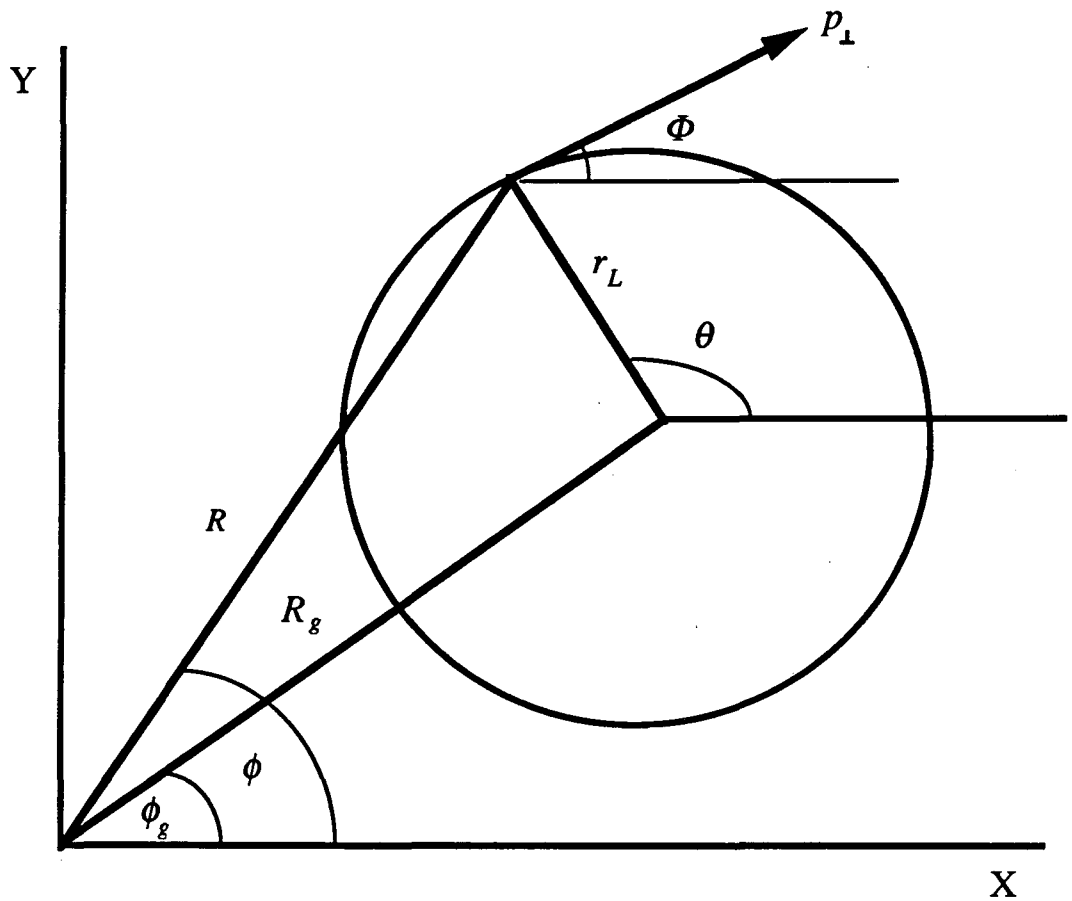

Fig.3b

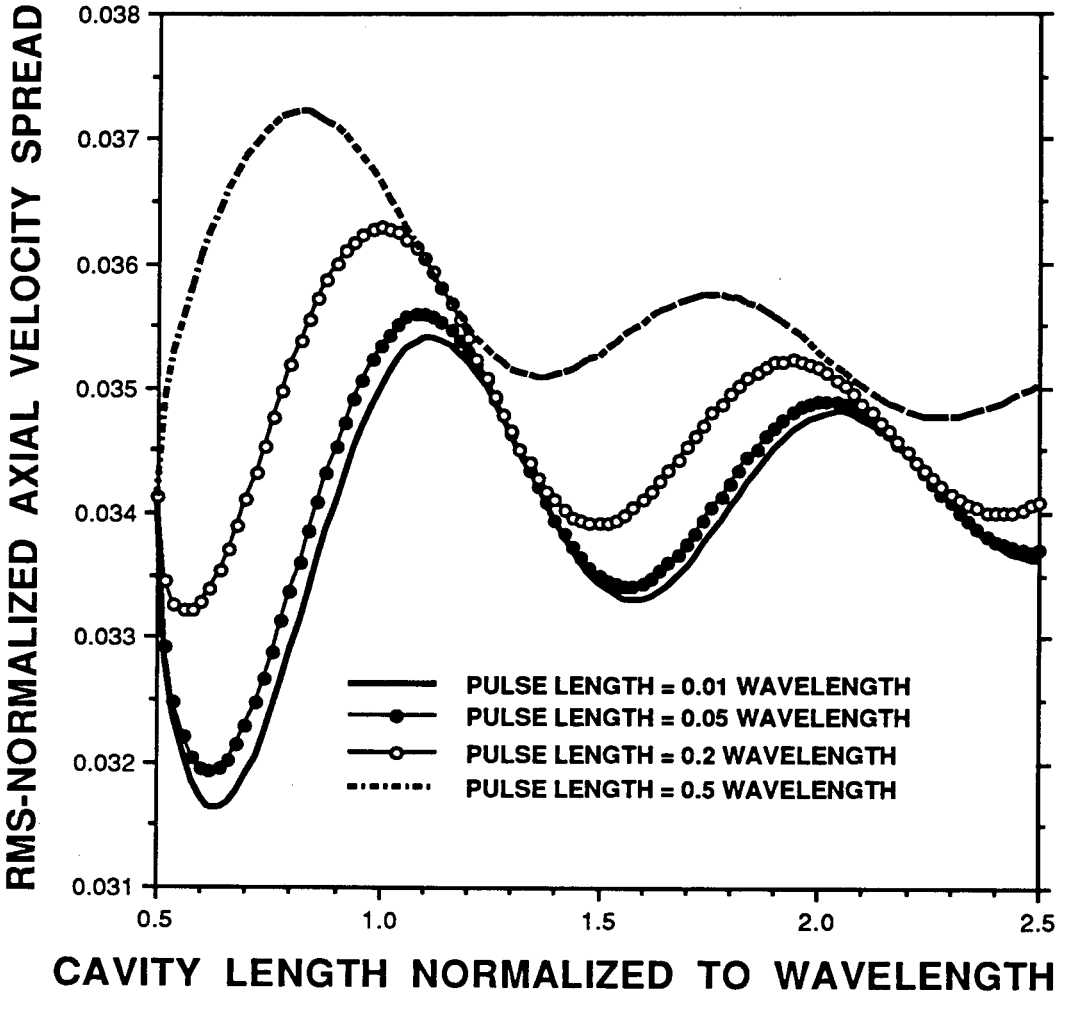
RMS-NORMALIZED AXIAL VELOCITY SPREAD
0.038
0.037
0.036
0.035
0.034
0.033
0.032
0.031
0.5
1.0
1.5
2.0
2.5
CAVITY LENGTH NORMALIZED TO WAVELENGTH
PULSE LENGTH = 0.01 WAVELENGTH
PULSE LENGTH = 0.05 WAVELENGTH
PULSE LENGTH = 0.2 WAVELENGTH
PULSE LENGTH = 0.5 WAVELENGTH

Fig.4

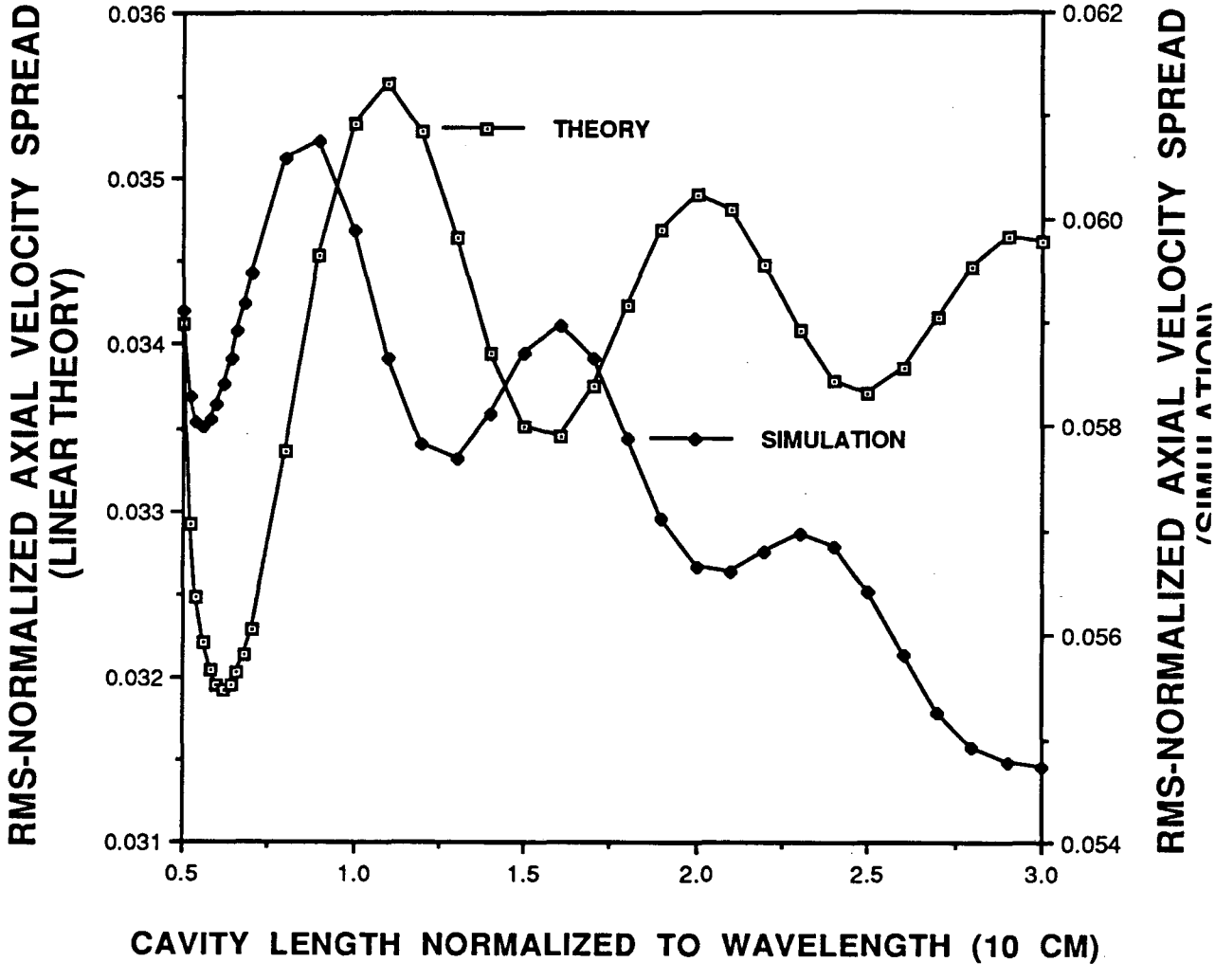
RMS-NORMALIZED AXIAL VELOCITY SPREAD
(LINEAR THEORY)
0.036
0.035
0.034
0.033
0.032
0.031
THEORY
SIMULATION
0.062
0.060
0.058
0.056
0.054
RMS-NORMALIZED AXIAL VELOCITY SPREAD
0.5
1.0
1.5
2.0
2.5
3.0
CAVITY LENGTH NORMALIZED TO WAVELENGTH (10 CM)

Fig.5

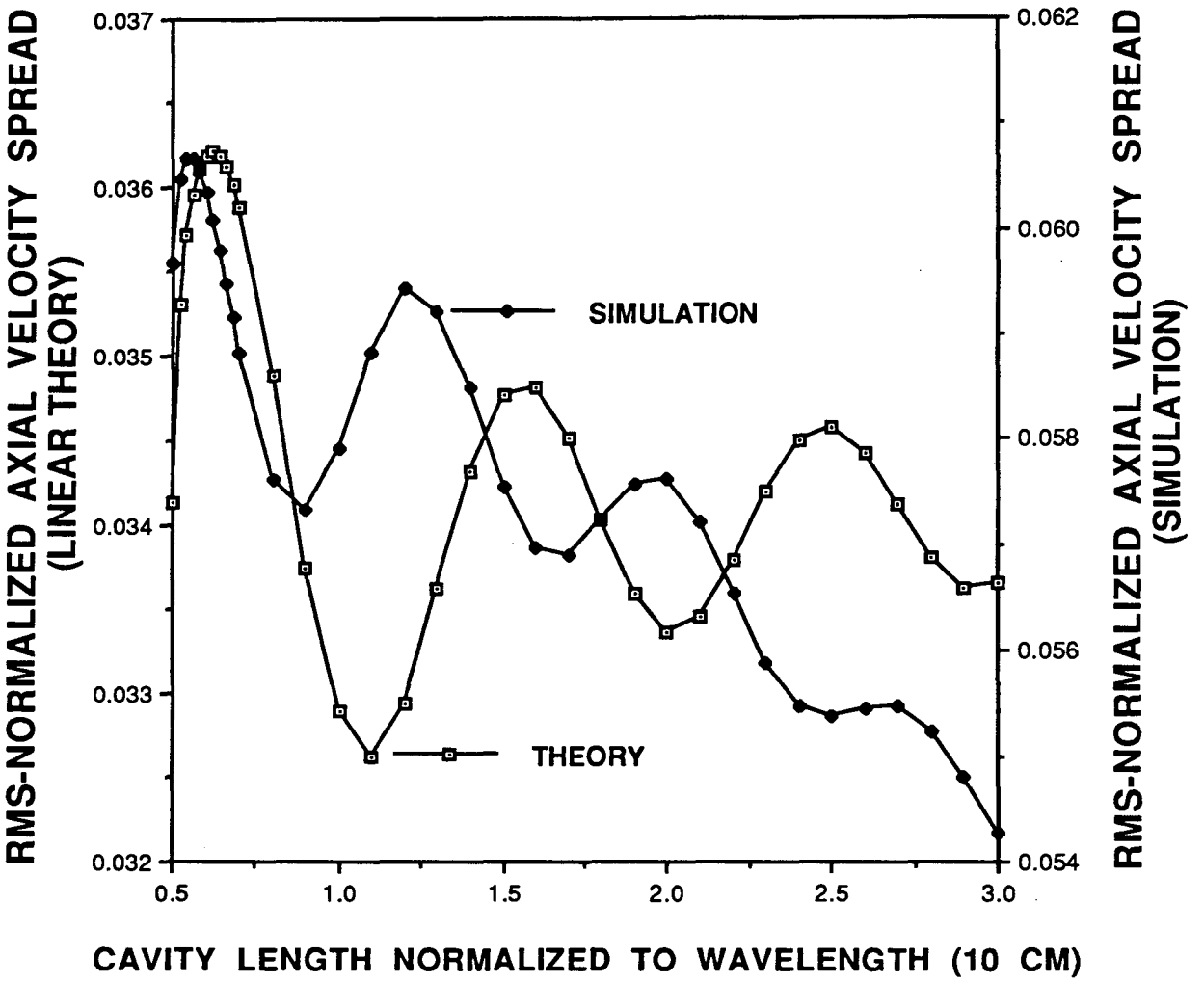
RMS-NORMALIZED AXIAL VELOCITY SPREAD
(LINEAR THEORY)
RMS-NORMALIZED AXIAL VELOCITY SPREAD
(SIMULATION)
0.037
0.036
0.035
0.034
0.033
0.032
0.062
0.060
0.058
0.056
0.054
0.5
1.0
1.5
2.0
2.5
3.0
SIMULATION
THEORY
CAVITY LENGTH NORMALIZED TO WAVELENGTH (10 CM)

Fig.6

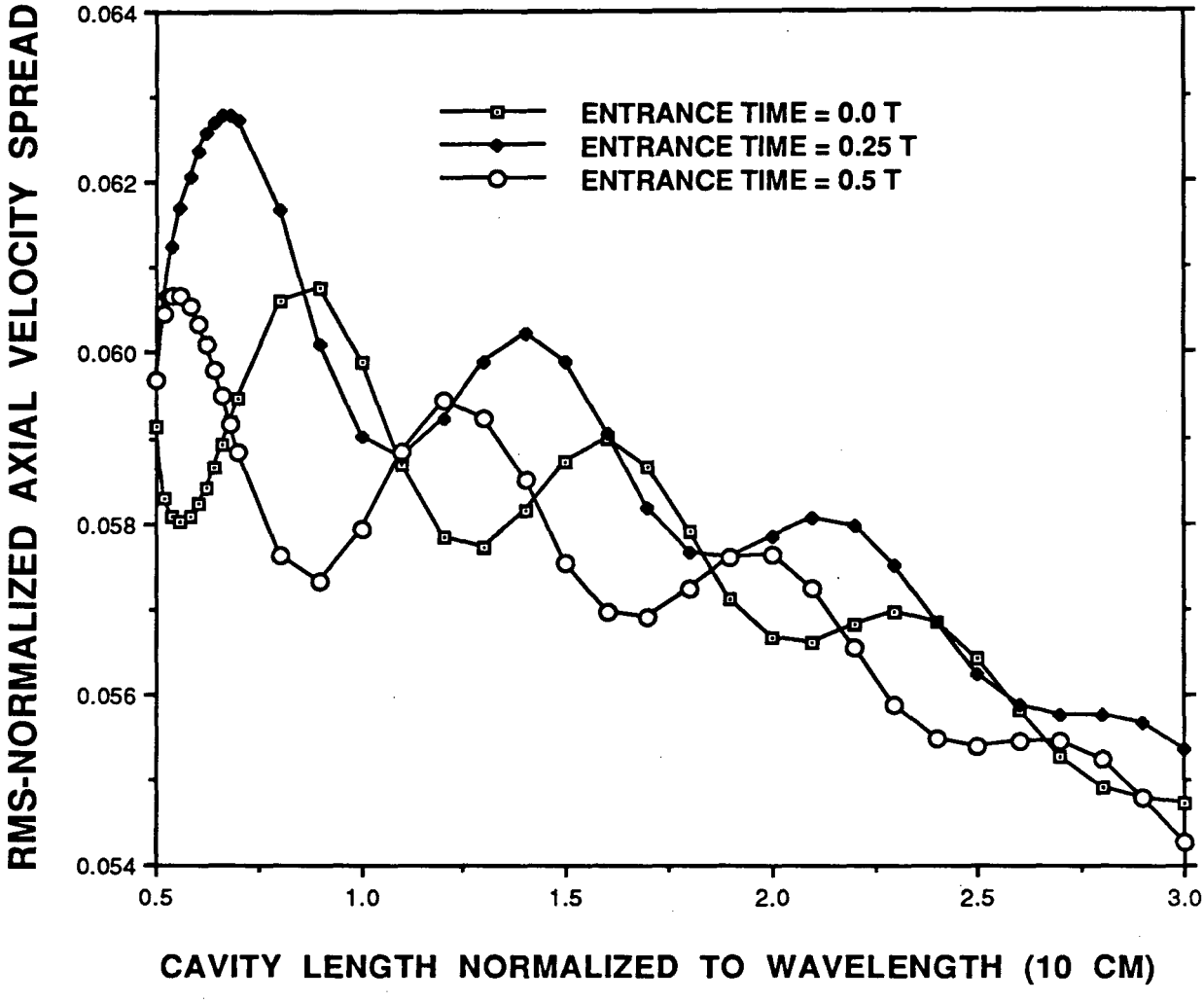
RMS-NORMALIZED AXIAL VELOCITY SPREAD
0.064
0.062
0.060
0.058
0.056
0.054
0.5
1.0
1.5
2.0
2.5
3.0
ENTRANCE TIME = 0.0 T
ENTRANCE TIME = 0.25 T
ENTRANCE TIME = 0.5 T
CAVITY LENGTH NORMALIZED TO WAVELENGTH (10 CM)

Fig.7

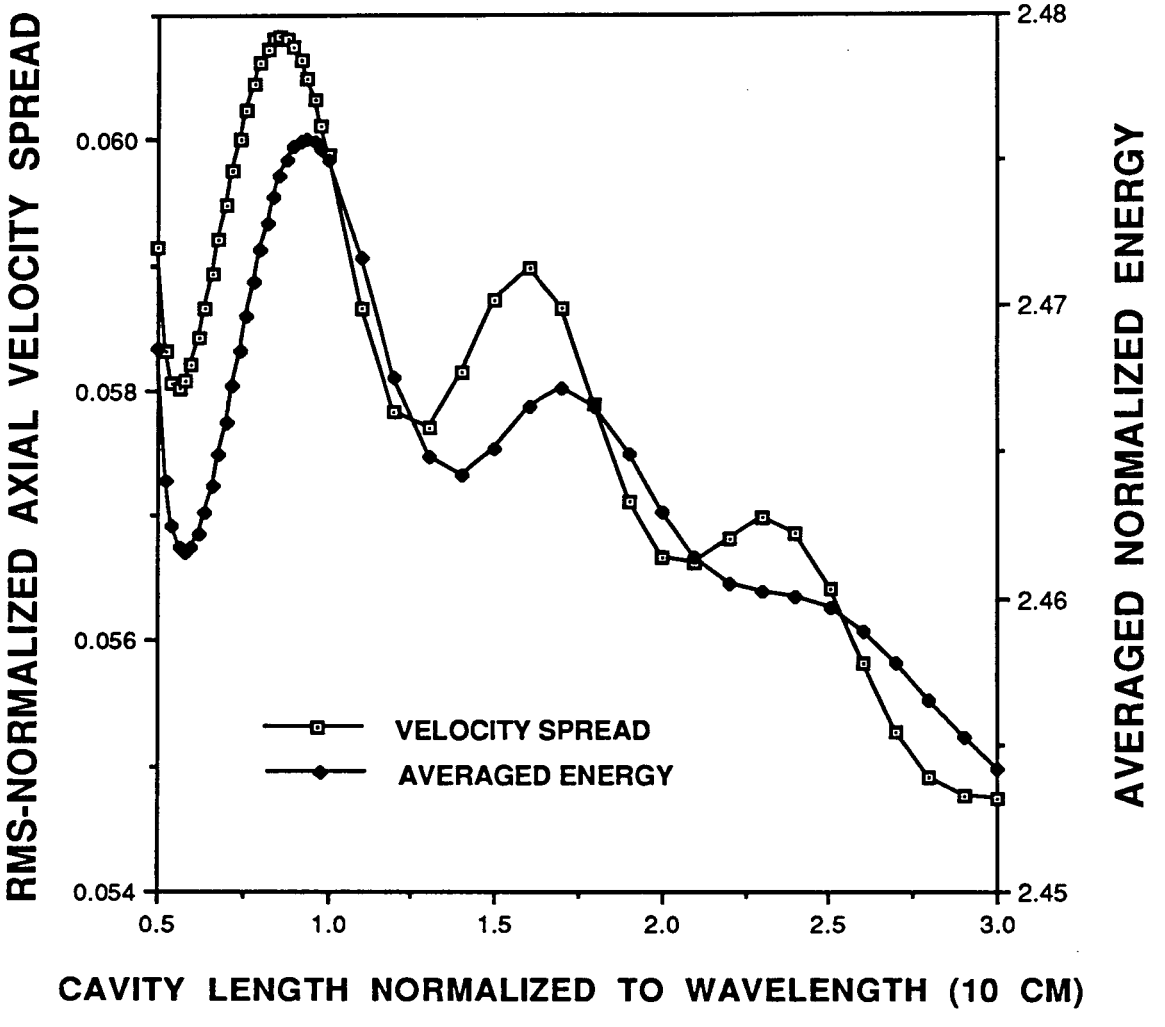
RMS-NORMALIZED AXIAL VELOCITY SPREAD
AVERAGED NORMALIZED ENERGY
0.060
0.058
0.056
0.054
2.48
2.47
2.46
2.45
0.5
1.0
1.5
2.0
2.5
3.0
VELOCITY SPREAD
AVERAGED ENERGY
CAVITY LENGTH NORMALIZED TO WAVELENGTH (10 CM)

Fig.8

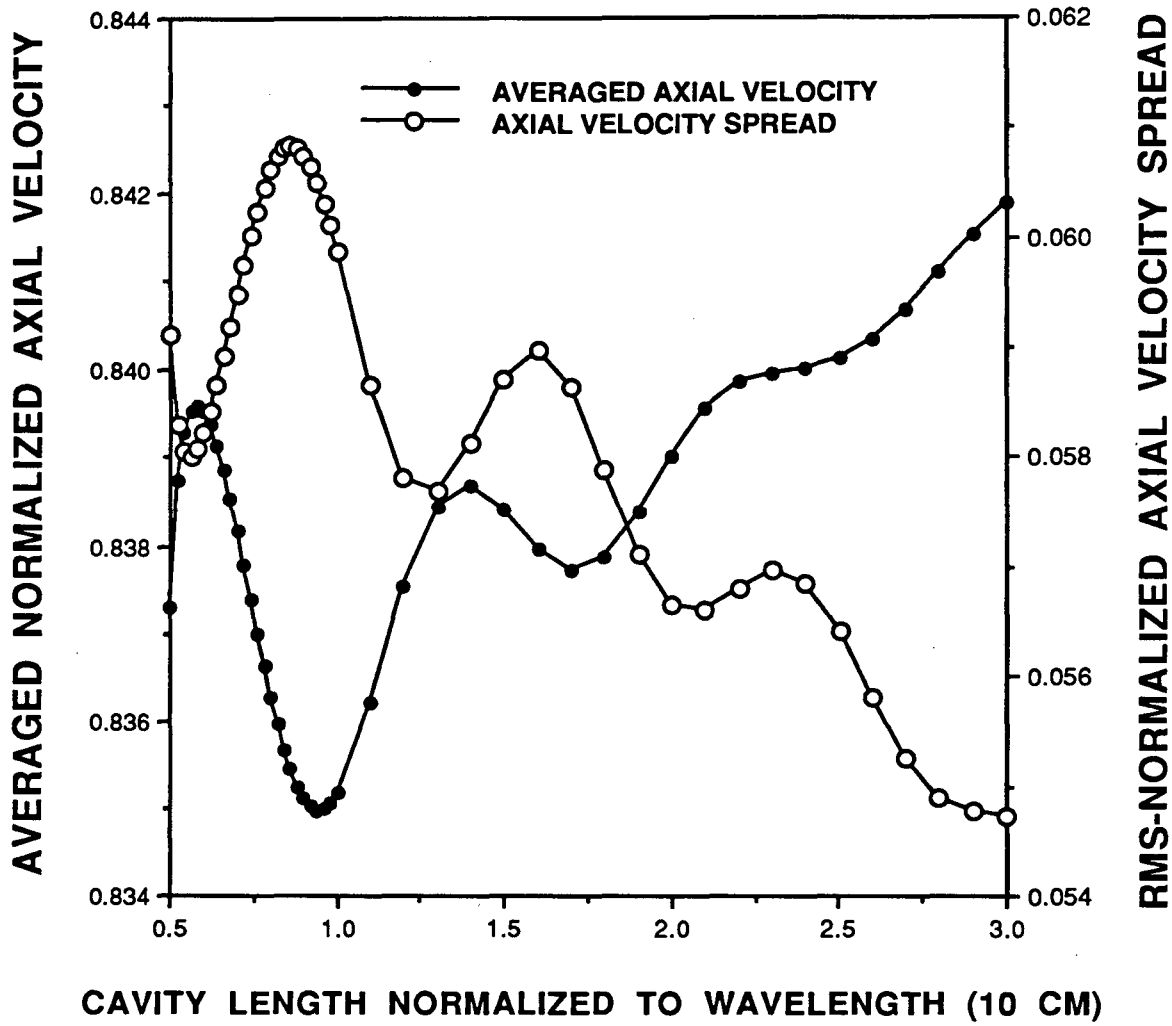
AVERAGED AXIAL VELOCITY
AXIAL VELOCITY SPREAD
AVERAGED NORMALIZED AXIAL VELOCITY
RMS-NORMALIZED AXIAL VELOCITY SPREAD
0.844
0.842
0.840
0.838
0.836
0.834
0.062
0.060
0.058
0.056
0.054
0.5
1.0
1.5
2.0
2.5
3.0
CAVITY LENGTH NORMALIZED TO WAVELENGTH (10 CM)

Fig.9

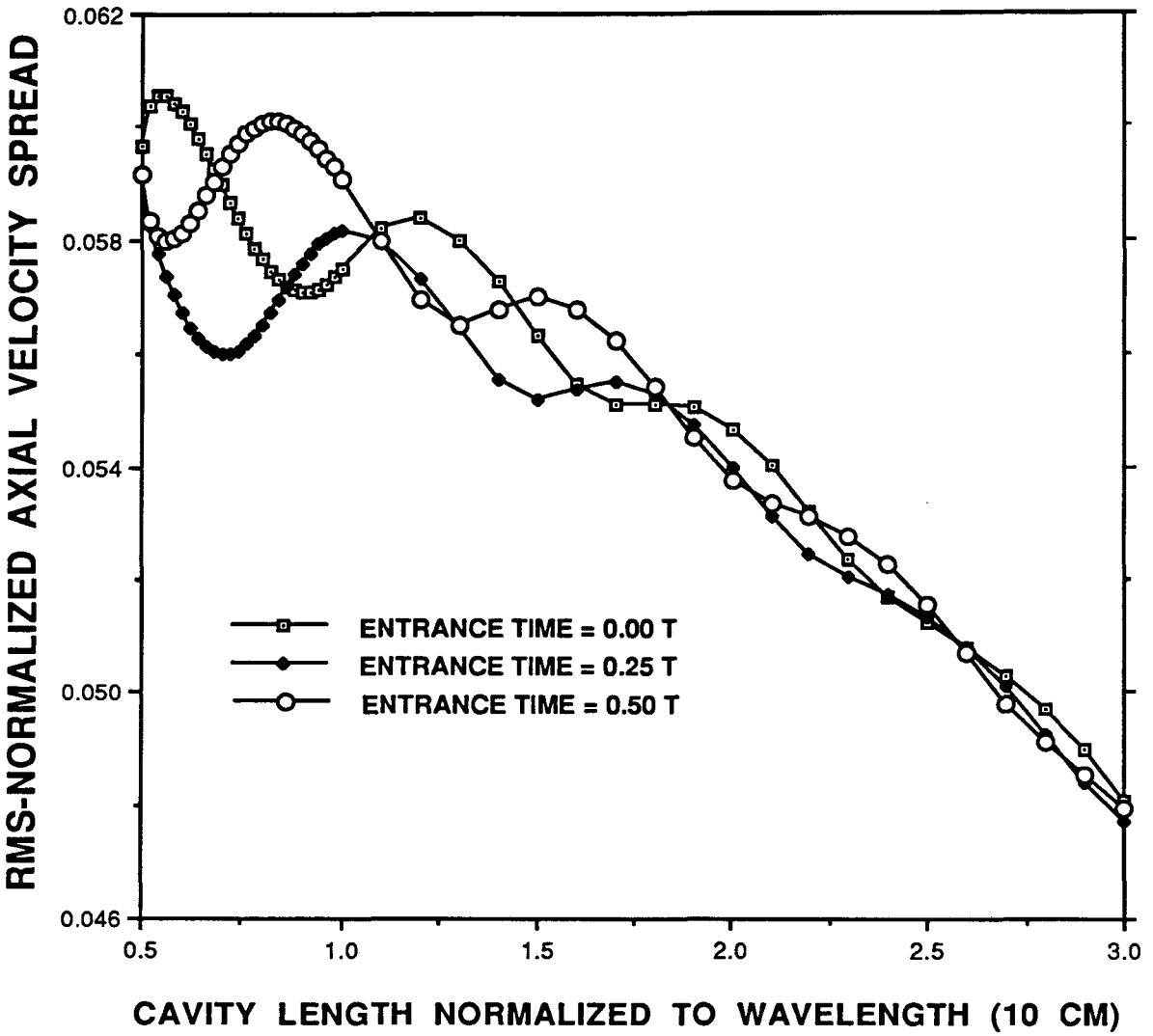
RMS-NORMALIZED AXIAL VELOCITY SPREAD
0.062
0.058
0.054
0.050
0.046
0.5
1.0
1.5
2.0
2.5
3.0
ENTRANCE TIME = 0.00 T
ENTRANCE TIME = 0.25 T
ENTRANCE TIME = 0.50 T
CAVITY LENGTH NORMALIZED TO WAVELENGTH (10 CM)

Fig.10a

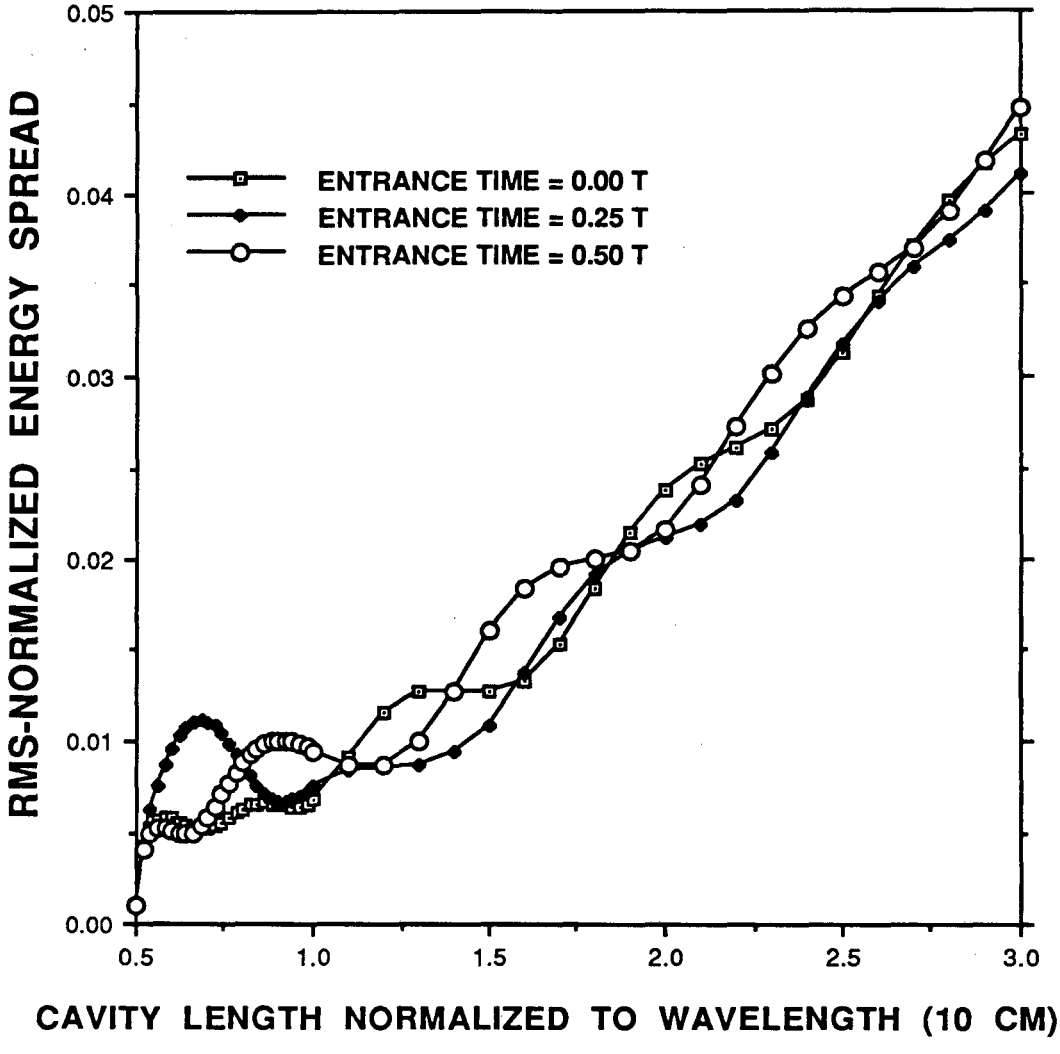
0.05
0.04
0.03
0.02
0.01
0.00
RMS-NORMALIZED ENERGY SPREAD
ENTRANCE TIME = 0.00 T
ENTRANCE TIME = 0.25 T
ENTRANCE TIME = 0.50 T
0.5
1.0
1.5
2.0
2.5
3.0
CAVITY LENGTH NORMALIZED TO WAVELENGTH (10 CM)

Fig.10b

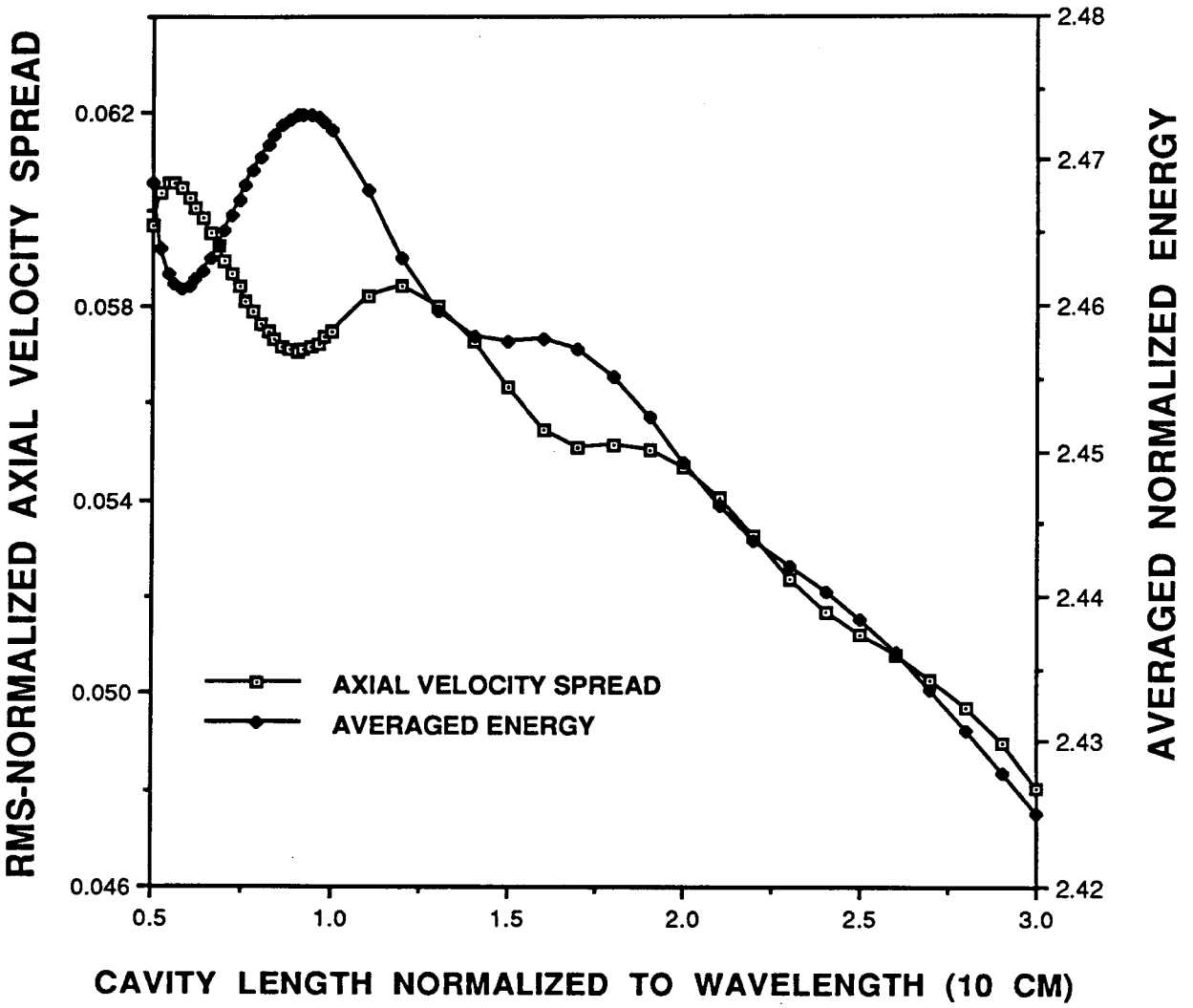
RMS-NORMALIZED AXIAL VELOCITY SPREAD
AVERAGED NORMALIZED ENERGY
0.062
0.058
0.054
0.050
0.046
2.48
2.47
2.46
2.45
2.44
2.43
2.42
0.5
1.0
1.5
2.0
2.5
3.0
AXIAL VELOCITY SPREAD
AVERAGED ENERGY
CAVITY LENGTH NORMALIZED TO WAVELENGTH (10 CM)

Fig.11

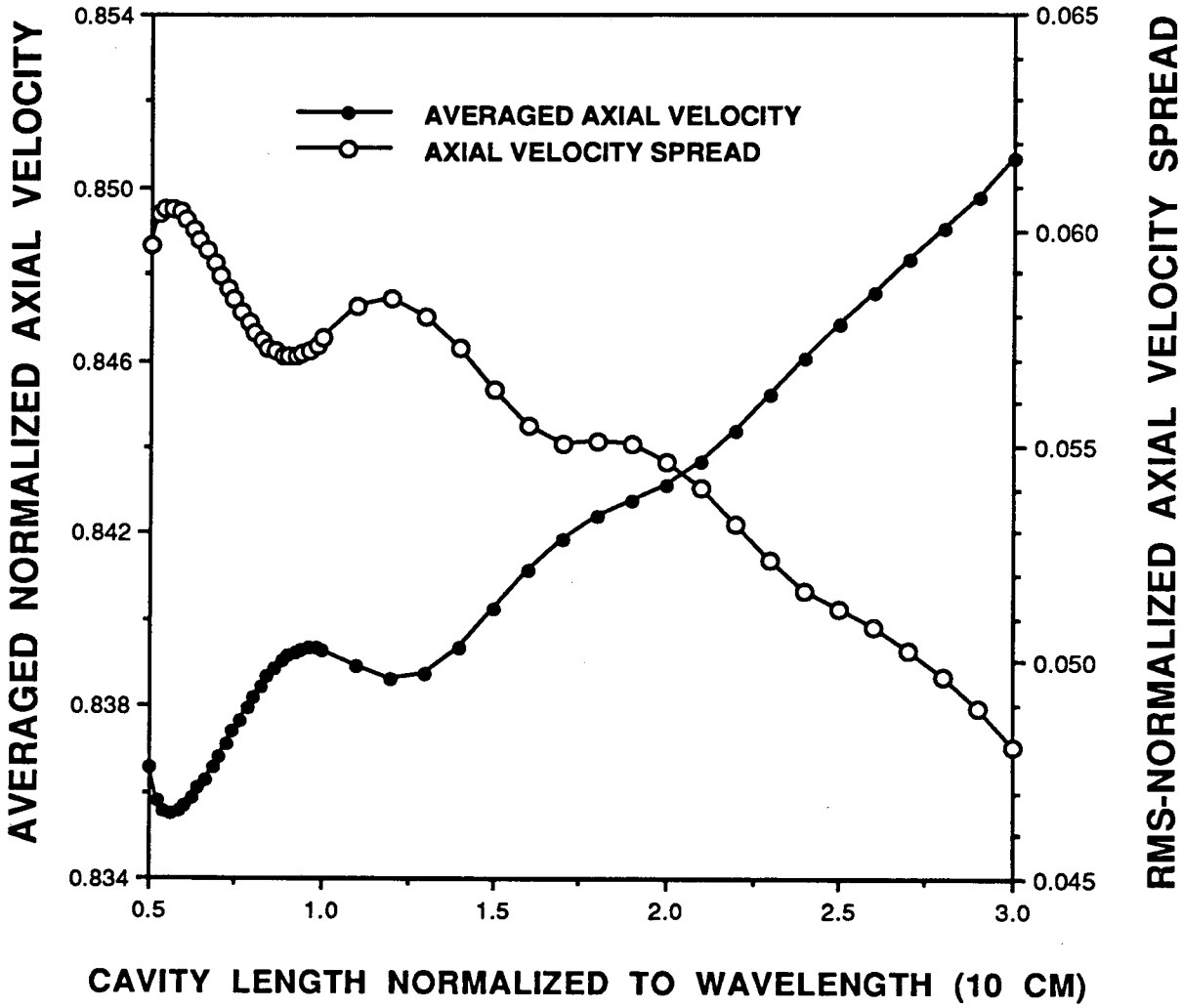
AVERAGED NORMALIZED AXIAL VELOCITY
RMS-NORMALIZED AXIAL VELOCITY SPREAD
AVERAGED AXIAL VELOCITY
AXIAL VELOCITY SPREAD
0.854
0.850
0.846
0.842
0.838
0.834
0.065
0.060
0.055
0.050
0.045
0.5
1.0
1.5
2.0
2.5
3.0
CAVITY LENGTH NORMALIZED TO WAVELENGTH (10 CM)

Fig.12

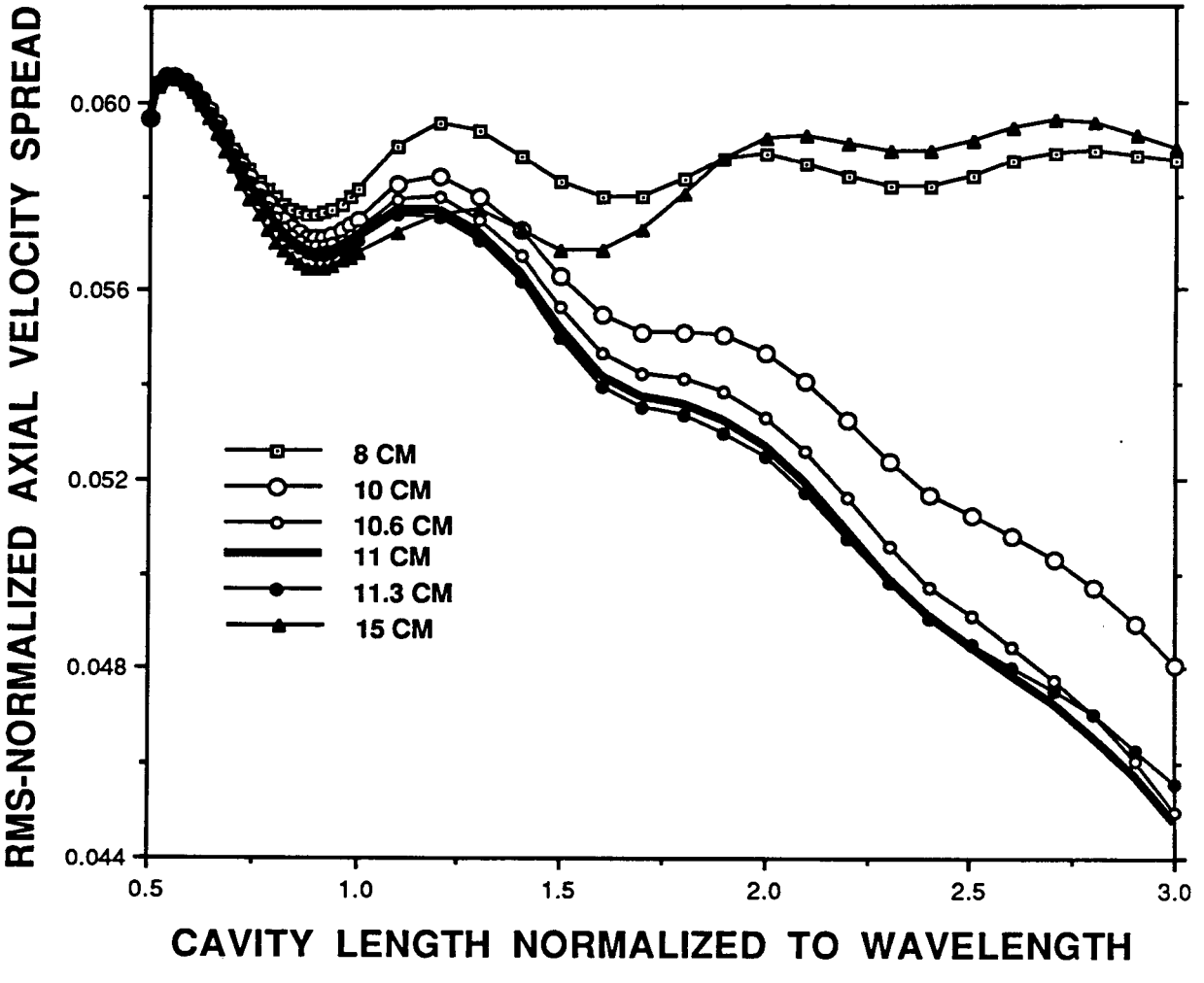
RMS-NORMALIZED AXIAL VELOCITY SPREAD
0.060
0.056
0.052
0.048
0.044
0.5
1.0
1.5
2.0
2.5
3.0
CAVITY LENGTH NORMALIZED TO WAVELENGTH
8 CM
10 CM
10.6 CM
11 CM
11.3 CM
15 CM

Fig.13

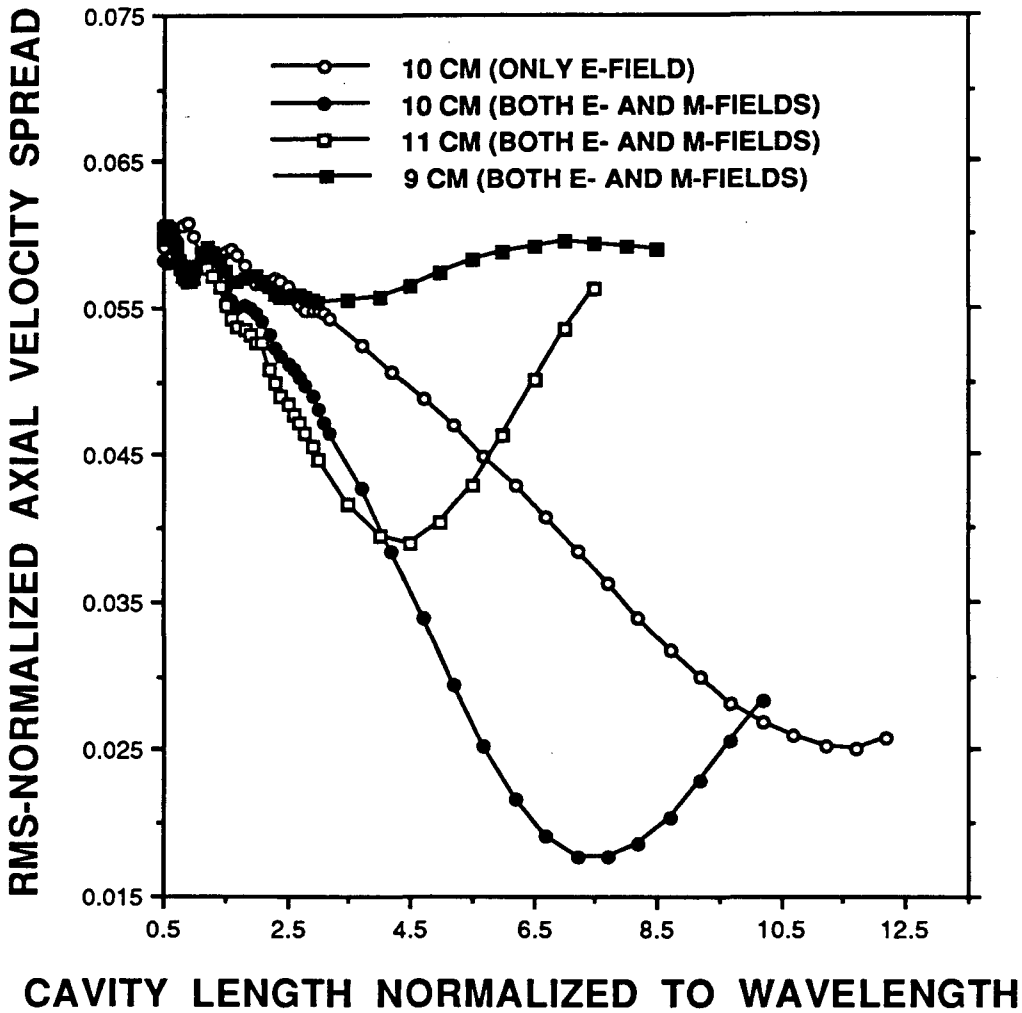
RMS-NORMALIZED AXIAL VELOCITY SPREAD
0.075
0.065
0.055
0.045
0.035
0.025
0.015
10 CM (ONLY E-FIELD)
10 CM (BOTH E- AND M-FIELDS)
11 CM (BOTH E- AND M-FIELDS)
9 CM (BOTH E- AND M-FIELDS)
0.5
2.5
4.5
6.5
8.5
10.5
12.5
CAVITY LENGTH NORMALIZED TO WAVELENGTH

Fig.14

LAWRENCE BERKELEY LABORATORY
UNIVERSITY OF CALIFORNIA
TECHNICAL INFORMATION DEPARTMENT
BERKELEY, CALIFORNIA 94720